SPIN-DOWN OF A STRATIFIED, ROTATING FLUID

by

ALAN D. ROBOCK

B.A., UNIVERSITY OF WISCONSIN

(1970)

SUBMITTED IN PARTIAL FULFILLMENT OF THE

REQUIREMENTS FOR THE DEGREE OF

MASTER OF SCIENCE

at the

MASSACHUSETTS INSTITUTE OF TECHNOLOGY

July, 1974

Signature of Author .....
Department of Meteorology, July 1974

Certified by .....
Thesis Supervisor

Accepted by .....
Chairperson, Departmental Committee
on Graduate Students

SPIN-DOWN OF A STRATIFIED, ROTATING FLUID

BY

ALAN D. ROBOCK

Submitted to the Department of Meteorology on 19 July 1974

in partial fulfillment of the requirements for the degree of

Master of Science

ABSTRACT

In this thesis a numerical model is used to study the spin-down of a stratified, rotating fluid. Simplified Boussinesq equations are used. The model results are compared to analytical results derived by imposing conditions on the one parameter, S, which appears in the non-dimensionalized equations, where $S = \sqrt{N^2 k^2/f^3}$. It is found that for small S, spin-down is dominated by Ekman pumping, with the model results corresponding to analytical results of an Ekman boundary layer beneath a quasi-geostrophic interior. For large S, the spin-down is dominated by diffusion of the interior flow, with boundary layers unimportant. This also corresponds to analytical results. Inertia-gravity waves are an important manifestation of the spin-down process for small S. Attempts are made to lessen their effects, so that the spin-down process itself may be studied. Applications to the real atmosphere and to the initialization of the boundary layer of numerical weather prediction models are studied.

Thesis Supervisor: Norman A. Phillips

Title: Professor of Meteorology

TABLE OF CONTENTS

LIST OF FIGURES

LIST OF FIGURES (continued)

LIST OF TABLES

SPIN-DOWN OF A STRATIFIED, ROTATING FLUID

I. Introduction

In this thesis, a numerical model is used to study the spin-down of a stratified, rotating fluid. Simplified Boussinesq equations are used. The model results are compared to analytical results derived by imposing conditions on the one parameter, S, which appears in the non-dimensionalized equations, where $S = \gamma N^2 k^2/f^3$. This study has applications to the boundary layer dynamics of the real atmosphere and to numerical weather prediction models.

Previous studies of this problem have been analytical and laboratory experimental. They have concentrated on the linear case of small relative angular velocities and small Ekman numbers ($E^{\frac{1}{2}}$ = ratio of Ekman depth to container depth) for a cylindrical laboratory vessel. Barcilon and Pedlosky (1967a) considered the case of E not small. In my case, due to the extreme simplifications of the equations and boundary conditions, the Ekman depth is incorporated in the non-dimensional parameter, S. Many of the results are the same. Greenspan and Howard (1963) were the first to study the problem for a neutrally stratified case. They defined three time scales that are important to the problem. Holton (1965) considered a slightly stratified case, corresponding to small S in my model, and showed how the analytical Ekman and quasi-geostrophic solutions matched his laboratory results.

Barcilon and Pedlosky (1967a) considered the highly stratified case, corresponding to large S in my model, and showed analytically that Ekman layers become unimportant in the spin-down of the interior, which is found to be controlled by diffusion. Later that year, Barcilon and Pedlosky (1967b) studied the complete range of the parameter S and showed how S as a function of E determined the type of motion present in the fluid. Benton and Clark (1974) give a complete review of all major work on the spin-up/spin-down problem.

II. Equations

A. Boussinesq Equations

The linearized, hydrostatic Boussinesq equations are used in this model. There is no basic current, no beta effect, uniform stratification, and uniform viscosity and conductivity. The perturbation equations are:

$$\left.\begin{aligned}
\frac{\partial u}{\partial t} - fv &= -\frac{\partial p}{\partial x} + \nu \frac{\partial^2 u}{\partial z^2} \\
\frac{\partial v}{\partial t} + fu &= \nu \frac{\partial^2 v}{\partial z^2} \\
\frac{\partial b}{\partial t} + N^2 w &= \nu \frac{\partial^2 b}{\partial z^2} \\
\frac{\partial p}{\partial z} &\simeq b \\
\frac{\partial u}{\partial x} + \frac{\partial w}{\partial z} &\simeq 0
\end{aligned}\right\} \qquad (1)$$

$\frac{\partial}{\partial y} = 0$; N^2, f and ν are constants.

N = Brunt-Vaisala frequency

$$N^2 = g \frac{d}{dz}\left(\frac{\bar{T} - T_a}{T_{a0}}\right) \approx \frac{g}{T}\left(\frac{g}{c_p} + \frac{\partial T}{\partial z}\right)$$

f = Coriolis parameter = $2\Omega \sin\phi$

γ = eddy viscosity coefficient

= eddy conduction coefficient

These are a very simple set of equations with many simplifying assumptions. This allows for a fairly simple numerical integration of the equations, while still retaining all the important physical aspects which are to be studied.

The region to be studied extends from $z = 0$ to $z = \infty$, with the following boundary conditions at $z = 0$: $u = 0$, $v = 0$, $w = 0$, $b = 0$. The initial conditions at $t = 0$ are: $u = 0$, $w = 0$, $b = 0$, and a barotropic, geostrophically balanced meridional velocity v:

$$v(x,z,0) = v_o \sin kx$$

$$p(x,z,0) = -(fv_o/k) \cos kx$$

$$v_o = \text{constant}$$

Because v has a constant, non-zero value at all z (except when $\sin kx = 0$), but $v = 0$ at $z = 0$, the viscosity and conductivity will immediately begin to change u, v, w, p and b. This is the spin-down process. It is as if at $t = 0$ a no-slip boundary condition is suddenly imposed at the bottom of a uniform current. This thesis will examine the flow fields produced during this spin-down process.

B. Non-dimensionalization

The equations and boundary conditions are such that each variable will maintain a single dependence on x, either $\sin kx$ or $\cos kx$. It is convenient to recognize

this explicitly and to select new variables as follows:

$$u = U(z,t) \sin kx$$
$$v = V(z,t) \sin kx$$
$$p = (f/k)\, P(z,t) \cos kx$$
$$b = (f/kD)\, B(z,t) \cos kx \qquad (2)$$
$$w = kD\, W(z,t) \cos kx$$

where: $z_{\text{dimensional}} = D\, z_{\text{non-dimensional}}$

$t_{\text{dimensional}} = (1/f)\, t_{\text{non-dimensional}}$

$D = \sqrt{\nu/f}$ = "Ekman depth"

Substituting (2) into (1) results in the following non-dimensional equations:

$$\frac{\partial U}{\partial t} - \frac{\partial^2 U}{\partial z^2} = V + P \qquad (3)$$

$$\frac{\partial V}{\partial t} - \frac{\partial^2 V}{\partial z^2} = -U \qquad (4)$$

$$\frac{\partial B}{\partial t} - \frac{\partial^2 B}{\partial z^2} = -SW \qquad (5)$$

$$\frac{\partial P}{\partial z} = B \qquad (6)$$

$$\frac{\partial W}{\partial z} = -U \qquad (7)$$

All the parameters collapse into one non-dimensional one:

$$S = \frac{D^2}{\lambda^2} = \frac{N^2 k^2 \nu}{f^3}$$

where $\lambda = f/Nk$ = "Prandtl or Rossby depth." Boundary conditions are:

$z = 0$: $U = V = W = B = 0$; all t (8a)

$z \to \infty$: $W, B \to 0$; U, V finite; all t (8b)

$$t = 0: \quad U = W = B = 0,\ V = 1;\ \text{all } z \tag{8c}$$

III. Theoretical Approximations for Small S

If the non-dimensional parameter S is small, approximate equations can be derived for an Ekman boundary layer, and a quasi-geostrophic interior. This is generally the case for mid-latitude synoptic scale motion. Reasonable values of the parameters in this case are: $\gamma = 10\ m^2\ sec^{-1}$, $k = 2\pi/4000$ km, $N^2 = 10^{-4}\ sec^{-2}$ and $f = 10^{-4}\ sec^{-1}$, and give $S = 0.0025$, which is small. In this case the Ekman depth, D, is 316 meters.

A. Ekman Equations

Assume a steady state ($\frac{\partial}{\partial t} = 0$), and that P is constant with height. This means that $\frac{\partial P}{\partial z} = 0$. Equation (6) then gives $B = 0$. Equation (5) then gives $SW = 0$, implying that S is small, since W is not ($W \sim O(1)$). The remaining equations then become:

$$-V = P + \frac{\partial^2 U}{\partial z^2} \tag{9}$$

$$U = \frac{\partial^2 V}{\partial z^2} \tag{10}$$

$$\frac{\partial W}{\partial z} = -U \tag{11}$$

with:

$$\left.\begin{aligned} &P = -V^* \\ &z \to \infty: \quad V = V^* \\ &z = 0: \quad U = V = W = B = 0 \end{aligned}\right\} \tag{12}$$

V^* is the quasi-geostrophic forcing from above and equals VQG (z=0), which will be defined in the next section.

Let $V' = V - V^*$. Equations (9-10) then become:

$$-V' = \frac{\partial^2 U}{\partial z^2} \qquad U = \frac{\partial^2 V'}{\partial z^2}$$

The solutions, using (12), are:

$$U = -V^* e^{-\sqrt{\frac{1}{2}}\, z} \sin \sqrt{\tfrac{1}{2}}\, z = UEK \tag{13}$$

$$V = V^* (1 - e^{-\sqrt{\frac{1}{2}}\, z} \cos \sqrt{\tfrac{1}{2}}\, z) = VEK \tag{14}$$

Integrating (11), and using (12) and (13):

$$W = \sqrt{\tfrac{1}{2}}\, V^* (1 - e^{-\sqrt{\frac{1}{2}}\, z}(\sin \sqrt{\tfrac{1}{2}}\, z + \cos \sqrt{\tfrac{1}{2}}\, z)) = WEK$$

As $z \to \infty$: $WEK \to \sqrt{\frac{1}{2}}\, V^*$.

B. Quasi-geostrophic Equations

In applying (3-7) to the interior, we ignore the viscous terms. We also know that $V = O(1)$ and, from the Ekman solution, that $W = O(1)$. By assuming quai-geostrophy, we have $P = O(1)$ and $\frac{\partial}{\partial t}$ small. Assigning symbolic magnitudes

$$\frac{\partial}{\partial t} = S^t \frac{\partial}{\partial t'},$$

$$\frac{\partial}{\partial z} = S^z \frac{\partial}{\partial z'},$$

$$U = S^u U'$$

$$B = S^b B'$$

we find that the symbolic power of S must satisfy

$$(3) \rightarrow \quad t + u > 0$$

$$(4) \rightarrow \quad t = u$$

$$(5) \rightarrow \quad t + b = 1$$

$$(6) \rightarrow \quad z = b$$

$$(7) \rightarrow \quad z = u\ .$$

These give, unambiguously, $u = b = z = t = \frac{1}{2}$, showing that the proper expansion is in powers of $S^{\frac{1}{2}}$. The resulting equations, when non-dimensionalized, are:

$$\left.\begin{array}{ll} \text{Zero order:} & V_0 = -P_0 \\ & U_0 = 0 \\ & W_0 = 0 \\ & B_0 = \frac{\partial P_0}{\partial z} \end{array}\right| \qquad \left.\begin{array}{ll} \text{First order:} & V_1 = -P_1 \\ & U_1 = -\frac{\partial V_0}{\partial t} \\ & W_1 = -\frac{1}{S}\frac{\partial B_0}{\partial t} \\ & B_1 = \frac{\partial P_1}{\partial z} \\ & U_1 = -\frac{\partial W_1}{\partial z} \end{array}\right\} \quad (16)$$

The matching condition on W is used as a lower boundary condition:

$$z = 0: \qquad W_1 = \text{WEK}\ (z \to \infty) = \sqrt{\tfrac{1}{2}}\, V^* \qquad (17)$$

Note that boundary conditions (8) apply to the zero order equations. Also note that $\frac{\partial U_1}{\partial t} \sim O(S)$ was neglected compared to $V_1 \sim O(\sqrt{S})$, a condition that S be small.

The potential vorticity equation can be derived from (16):

$$\left(\frac{\partial^2}{\partial z^2} - S\right)\frac{\partial P_0}{\partial t} = 0$$

This equation is solved using conditions (8) and (17):

$$\left.\begin{array}{l} P_0 = v_0\, e^{-\sqrt{S}\, z}\,(1 - e^{-\sqrt{S/2}\, t}) - v_0 \\ \text{where } v_0 = V^*\ (t=0) \end{array}\right\} \quad (18)$$

Letting $v_0 = 1$, putting (18) back into (16), and dropping subscripts, the quasi-geostrophic equations are:

$$
\left.
\begin{aligned}
V &= 1 - e^{-\sqrt{S}\, z}\,(1 - e^{-\sqrt{S/2}\, t}) = VQG \\
W &= (1/\sqrt{2})\, e^{-\sqrt{S}\, z}\, e^{-\sqrt{S/2}\, t} = WQG \\
U &= (\sqrt{S}/2)\, e^{-\sqrt{S}\, z}\, e^{-\sqrt{S/2}\, t} = UQG \\
P &= -V \\
B &= -\sqrt{S}\, e^{-\sqrt{S}\, z}\,(1 - e^{-\sqrt{S/2}\, t})
\end{aligned}
\right\} \qquad (19)
$$

These equations all satisfy (8) for zero order, but the U and W equations here are really for first order.

IV. Theoretical Approximation for Large S - Diffusion

If S is large, approximations can be made which result in a diffusion equation. Equations (5) and (7) suggest that W and U are small, and that (4) reduces to:

$$\frac{\partial V}{\partial t} - \frac{\partial^2 V}{\partial z^2} \approx 0 \qquad (20)$$

With the boundary conditions

$z = 0$: $V = 0$; all t

$z \to \infty$: $V = 1$; all t

$t = 0$: $V = 1$; all z,

this is Stokes' first problem. The solution, according to Hildebrand (1962, pp. 462-464) is:

$$V = \operatorname{erf}\left(\frac{z}{2\sqrt{t}}\right) \qquad (21)$$

where $\operatorname{erf}(x) = (2/\sqrt{\pi}) \int_0^x e^{-u^2}\, du$, is the so-called error function, whose values are tabulated.

V. Results

The numerical model used in this study is described in the Appendix. The results of the runs made with this model are presented in this section.

A. Inertia-Gravity Waves and the Lid

Inertia-gravity waves are produced in this model by the sudden imposition of friction at the bottom boundary. They are not filtered out by the equations. An equation for the frequency of these inertia-gravity (I-G) waves was derived. By combining equations (3-7), the following equation was derived for W:

$$\frac{\partial^6 W}{\partial z^6} - 2\frac{\partial^5 W}{\partial t\,\partial z^4} + \frac{\partial^4 W}{\partial t^2 \partial z^2} + \frac{\partial^2 W}{\partial z^2} - SW = 0$$

If W is considered to vary exponentially in time and height:

$$W = w_o\, e^{i(\gamma z + \omega t)},$$

the following equation is derived for the frequency of the I-G waves:

$$\omega = \pm \frac{1}{\gamma}\sqrt{\gamma^2 + S} + \gamma^2 i$$

where $\gamma = n\pi/H$, $n = 1, 2, 3, \ldots$

The first term in the frequency equation gives the frequency of the periodic variations of the I-G waves and the second term gives the exponential decay of the amplitude due to viscosity. The period of the I-G waves is given by:

$$\tau = \frac{2\pi}{Re\ \omega}$$

A series of twelve runs were conducted to study these

waves as a function of S and H. Graphs of the resulting W are given in Figures 1-12, and the results are summarized in Table 1, which also contains a summary of all runs made in this study. Runs were made for H varying from 7.9 to 63.2, corresponding to a dimensional height ranging from 5 km to 20 km when $f = 10^{-4}$ sec^{-1} (mid latitudes) and $\nu = 10$ m^2 sec^{-1}, with S varying from 0.4 to -0.01, thus testing the model for neutral and unstable cases as well.

In Runs 1-11 (Figures 1-11), n = 1 I-G waves were observed with periods corresponding to theoretical predictions. In Run 11, I-G waves were present even for an unstable stratification, because the instabilities were effectively damped by viscosity. In Run 12 (Figure 12), W increased exponentially for the whole run, with no waves, as was predicted. In Run 2, n = 2 waves appear to dominate, as the period of the n = 1 waves becomes small. When the period of the n = 1 I-G waves is below a certain critical value, $\tau_c \approx 2$, higher mode waves begin to appear. As S and H are increased, not only does the frequency of the I-G waves increase, but the higher mode waves are relatively larger (See Figure 2). Note that the n = 1 mode in W is dominant at z = H/2; the n = 2 mode is more apparent at z = H/4 and z = 3H/4, especially in Figures 2 and 4.

Runs 5-8 (Figures 5-8) with S = 0.01, and H varying from 7.9 to 63.2 Ekman depths, show that for $t \leq 14$ the region below z = 16 is little affected by increasing H above a value of 16. Nonetheless, H = 63.2 was used as a

standard height for most later runs. One systematic occurence shown in Figures 5-8 is the tendency, at $z > 5$, to a second maximum in W at t somewhat greater than the pure inertia period 2π, approaching closer to 2π from above as H is increased.

It should be noted, however, that while the I-G waves markedly affected the U and W fields, the V fields were much less affected, since the change in V from the initial value of 1 in a sense corresponds to the time integral of U (Compare Figure 8 for W and Figure 15 for V). As S became larger, as in Runs 13 and 14 (Figures 26, 27 and 33, 34), the U and W fields became much less important as compared to the V field, so that even though the I-G wave structure became more complex, it has less observable effect on the V field. For a small S, however, the I-G waves affect the V field to some extent, and it would be nice to find a way to suppress them, so the spin-down process could be studied unaffected by them.

B. Boundary Layer and Wmax

As can be seen in Figures 1-11, a boundary layer develops in W. W grows from 0 to a maximum at a certain z and t, and then after that in time, Wmax is at a somewhat lower height. Data related to this was taken from these figures and later runs, and tabulated in Table 2, and plotted in Figures 13-14.

Figure 13 shows that there is a linear relationship between the first Wmax (d) and its height (a):

$a \approx 1.65 + 3.75d$. This is true independent of S or H, although the first Wmax and its height both tend to decrease with increasing S. Figure 14 shows an almost linear relationship between the first Wmax (d) and the time of its occurence (c): $c \approx 0.9 + 3\ d$. Wmax tends to stay at slightly less than the height of the first Wmax (Compare columns a and b in Table 2), and to decay slowly quasi-exponentially in magnitude.

C. Small S (0.01)

Run 8 (S = 0.01, H = 63.2) was used as a standard small S case to be compared with Run 13 (S = 0.16, H = 63.2), a case of moderate S, and Run 14 (S = 2.56, H = 63.2), a case of large S. Figures 15, 16 and 8 contain plots of V, U and W for Run 8. Theoretical Ekman and quasi-geostrophic plots, using equations (13, 14 and 19) and setting $V^* = e^{-\sqrt{S/2}\ t}$, were also made for Run 8 and are shown in Figures 17-22.

It can be seen in Figure 15 that initially an Ekman-like boundary layer is established near the surface and then Ekman pumping and associated U flow (See Figure 16) produce a quasi-geostrophic-like spin-down of the interior flow. Figure 15 shows the establishment of the Ekman layer of Figure 17. Figure 20, if raised one Ekman depth, shows close correspondence of the numerical results to the quasi-geostrophic solution. The U and W plots, Figures 16 and 8, resemble the Ekman plots, Figures 18 and 19, near the surface. However the quasi-geostrophic plots, Figures 21 and 22, show rough agreement with the numerical results

only when raised up about four units in z. If the Ekman and quasi-geostrophic solutions were summed, the model results would probably resemble this sum near the bottom boundary, while the I-G waves in the interior would cause the two plots to be different.

An attempt was made to start the model with different, more balanced initial conditions, so that there would be less of a shock to the system and smaller amplitude I-G waves resulting. This was done in Run 15, where the following initial conditions were used instead of (8c):

$t = 0$: $U = UEK + UQG$

$V = VEK$ (which includes VQG)

$B = 0$

The UEK and VEK components are a reasonable boundary layer structure for VQG, however the UQG component does not have a boundary layer and does not satisfy the boundary condition on U at $z = 0$. The results are plotted in Figures 23-25. Comparing these results to those for Run 8 (Figures 15, 16 and 8), it can be seen that the attempt was only partly successful. Comparing the V fields, in Run 15 the spin-down of the interior is slightly more rapid than that in Run 8, since the boundary layer and counterflow have already been established at $t = 0$. Some oscillations still occur, but with less influence.

An earlier attempt starting with an Ekman profile for U and V without the quasi-geostrophic adjustment in U resulted in similar fields to those of Runs 8 and 15, but

with larger I-G wave amplitude. An attempt starting with combined Ekman and quasi-geostrophic profiles, except with the quasi-geostrophic profiles moved up one Ekman depth, or: $t = 0$: $U(z) = UEK(z) + UQG(z+1)$, gave results almost identical to those of Run 15.

A run was also made with a boundary layer structure for UQG so that the initial U field satisfied the boundary condition at $z = 0$. The following profiles were derived from the paper by Young (1973) for the isallobaric flow in the boundary layer, since my UQG is just the isallobaric wind:

$$UIB = U^* \left\{1 - e^{-\sqrt{\frac{1}{2}}\, z}\left[\cos \sqrt{\tfrac{1}{2}}\, z + (z/\sqrt{8})(\sin \sqrt{\tfrac{1}{2}}\, z + \cos \sqrt{\tfrac{1}{2}}\, z)\right]\right\}$$

$$VIB = U^* e^{-\sqrt{\frac{1}{2}}\, z}\left[\sin \sqrt{\tfrac{1}{2}}\, z + (z/\sqrt{8})(\sin \sqrt{\tfrac{1}{2}}\, z - \cos \sqrt{\tfrac{1}{2}}\, z)\right]$$

$U^* = UQG\ (t = 0)$. The initial conditions for this run were then:

$$U = UEK + UIB$$

$$V = VEK + VIB$$

where UEK and VEK are the boundary layer corrections for VQG, and UIB and VIB are the boundary layer corrections for UQG. The results were again almost identical to those of Run 15. The Ekman boundary layer correction to the zero-order quasi-geostrophic V field, therefore, appears to be important, while the boundary layer correction to the first-order quasi-geostrophic U field does not have a large effect.

D. Moderate S (0.16)

Run 13 was the same as Run 8, except that $S = 0.16$ in Run 13 (0.01 in Run 8). Model results for V and U are

plotted in Figures 26 and 27, and Ekman and quasi-geostrophic theoretical results are plotted in Figures 28-31.

In this case, $\sqrt{S}$ is not very small compared to 1. The theoretical results valid for small S, therefore, would not be expected to be good estimates for this case. The V field (Figure 26) spins down more slowly than the VEK (Figure 28) and the VQG (Figure 30) fields. The U field (Figure 27) also spins down more slowly than the UEK field (Figure 29) beyond $t \approx 8$, but again it is hard to compare to the UQG field (Figure 31) because boundary conditions are not satisfied.

Neither is S large enough in this case to be "large." The V profile of equation (21), for the theoretical large S case, is shown in Figure 32. When this is compared to Figure 26, it is seen that while after $t \approx 4.5$, the two profiles have the same shape, the V for moderate S has spun down more rapidly than the diffusive solution for V.

The "jet" of positive U above the boundary layer in Figure 27 is the interior divergence caused by the Ekman pumping. A jet of magnitude greater than 0.05 is evident from $t \approx 1$ to $t \approx 4.5$ in Figure 27, and the results of this pumping are seen in Figure 26. Between $t \approx 1$ and $t \approx 4.5$ in the V field a structure is observed similar to that in the V field for Run 8 (Figure 15), caused by the Ekman pumping. But after this time the pumping decreases, a diffusion type regime is observed for V, and the weak boundary layer formed at the beginning of the run disappears.

E. Large S (2.56)

Run 14 was the same as Run 8, except that S = 2.56 (0.01 in Run 8). Numerical results for V and U are plotted in Figures 33 and 34, and UEK and VQG are plotted in Figures 35 and 36.

There is almost no resemblance between the numerical results for large S and the theoretical results based on small S. Only a diffusive regime is present in the V field, with no boundary layer structure, and it is in fact almost identical to the theoretical diffusive result of equation (21) and Figure 32. The U flow is much smaller than when S is small.

F. Dimensional Results

This section considers the physical meaning of varying S. S is a function of four parameters: γ, N, k and f. Each in turn is varied while the other three are held constant and the variation of S is interpreted as a dependence on each of the parameters individually. This was done by assuming that for S = 0.01; $\gamma = 10\ m^2\ sec^{-1}$, $N = 10^{-2}\ sec^{-1}$, and $f = 10^{-4}\ sec^{-1}$, corresponding to a latitude of 43^{o}. The horizontal wave number k was then calculated and found be $3.16 \times 10^{-6}\ m^{-1}$. This gives a horizontal wave length of 2000 km. This is a minimum wave length for the small S case. As the wavelength is increased to values more closely corresponding to those observed in mid latitudes, S becomes smaller and the theoretical results for small S will fit the model results even better.

N does not appear in the scaling of the independent and dependent variables in equations (3-7). Therefore, comparisons based on variations in N imply only a change in S without changes in z, t or the fluid variables. The plots already constructed may be used for comparison directly. The scaling does depend, however, on the other three parameters. Care must be taken so that when they are varied, the scaling definitions are accounted for. In the following discussion the above values will be taken as a reference; changes in each one of the four parameters will be considered in turn in terms of changes in S and spin-down process which it produces.

1. Varying f

Holding N, ν and k constant at the reference values given above, dimensional height and time scales have been placed on Figure 15 (V, S = 0.01, f = 10^{-4} sec^{-1}). Figures 37 and 38 are dimensional plots of V for S = 0.16, f = 4×10^{-5} sec^{-1} (17 degrees latitude) and for S = 2.56, f = 1.6×10^{-5} sec^{-1} (6 degrees latitude) on the same scale as the dimensional coordinates of Figure 15. The following analysis is valid only in the planetary boundary layer, where the Boussinesq approximation is valid, and only when other characteristics of the real atmosphere not considered here, such as latent heat, are unimportant.

Below 1 km, and for time less than 1 day the spin-down is most rapid for a large S and slowest for small S. Between 1 km and 2 km, however, the character of the profiles

changes dramatically. For small S, V actually decreases momentarily with height in this region, and for moderate S, $\left|\frac{\partial V}{\partial z}\right|$ decreases substantially from the larger values near the ground. For large S, $\left|\frac{\partial V}{\partial z}\right|$ simply decreases gradually with height. The net result is that at z = 2 km, the small S case has spun down the most and the large S case has spun down the least. The Ekman pumping, which has its greatest effect in the 1-2 km region, dominates in the small S case, causing a rapid spin-down, while in the large S case, pumping is almost absent, and diffusion is the dominant mechanism of spin-down. This is shown explicitly by the dimensional plots of Wmax versus t(Wmax) in Figure 14: the larger S is, the longer it takes for Wmax to be reached and the smaller is its magnitude. Since Wmax is an indication of the magnitude of the Ekman pumping, this again indicates that pumping is much more important for small S than for large S as a spin-down mechanism. The moderate S case is a transition between these two extremes.

Further evidence for diffusion dominating in the large S case is a comparison of the dimensional V profile (Figure 38) with the non-dimensional profile (Figure 33). The shape and spacing of the iso-lines is almost exactly the same, indicating that V is a function of the ratio of the coordinate scaling. Since z is scaled by $f^{-\frac{1}{2}}$ and t by f, V must be a function of $z/\sqrt{t}$. This is the case for pure diffusion (See equation (21)).

It can be concluded then, subject to the above

restrictions, that in mid and high latitudes Ekman pumping dominates spin-down, while in low latitudes diffusion causes spin-down. One other factor which might negate this conclusion is that f varies rapidly in the low latitudes, while in the equations it was assumed to be constant.

2. Varying ν

If the results are interpreted by varying ν and keeping f, k and N constant as S changes, the effect of viscosity may be studied. As would be expected, as ν and S are increased diffusion becomes more important and dominates. For small ν, Ekman pumping dominates. S is directly proportional to ν, so as S is varied by a factor of 256, so is ν. This would vary the vertical scaling by $\nu^{\frac{1}{2}} = 16$, but not affect the time scaling. If ν is taken as a reasonable atmospheric value for small S, then for large S, both ν and the vertical scaling become unreasonable. This makes sense since an "Ekman depth" = $(\nu/f)^{\frac{1}{2}}$ would not be a reasonable scaling when there is no Ekman layer and the spin-down is dominated by diffusion, as is the case for large S.

3. Varying N

If N is varied with S, and f, ν and k are kept constant, these results verify those of Barcilon and Pedlosky (1967a). As the stability is increased, N goes up and so does S. This produces a viscous spin-down, because increased stability inhibits vertical motion and therefore inhibits Ekman pumping. The large S case, however, involves unrealistically large values of N for the atmosphere ($dT/dz \approx$

+ 1000 degrees/km).

4. Varying k

An increase of k with S corresponds to a decrease in wavelength of the horizontal forcing of the motion. This indicates that for small scale motions, diffusion becomes dominant over pumping as the spin-down mechanism. If L = 2000 km for the small S case, then the large S case corresponds to L = 125 km. This indicates that spin-down in meso-scale and smaller scale disturbances in mid latitudes is dominated by diffusion.

VI. Conclusions

Spin-down of a stratified, rotating fluid is studied with a numerical model. For a case of small S (0.01), Ekman pumping is found to be the dominant spin-down mechanism. The resulting flow closely resembles an analytical solution of a quasi-geostrophic interior with an Ekman boundary layer. For a case of large S (2.56), diffusion is the dominant spin-down mechanism. The resulting flow closely resembles a purely diffusive analytical solution to Stokes' first problem. A case of moderate S (0.16) is a transition between the above two extremes, and exhibits characteristics of both Ekman pumping and diffusive spin-down.

When realistic atmospheric values of the parameter S are introduced, it is found that the small S case corresponds to mid and high latitude motion with large-scale

horizontal forcing. The large S case corresponds to low latitudes, or to meso- and smaller scale horizontal forcing.

Inertia-gravity waves are an important manifestation of the spin-down process for small S. A partially successful method is devised to lessen their effects. This has applications in initialization of numerical weather prediction models.

VII. Figures and Tables

Figures and tables refered to in the text follow this description. Diagrams of W have a different $\tilde{z}_\Lambda$ scale than those of V and U, as they are compacted so the entire field can be studied for I-G waves. Figures with a dashed (- - - -) upper boundary do not include the upper portion of the data, as only the region near the ground is of interest. Coordinates marked "z" refer to non-dimensional height and those marked "t" refer to non-dimensional time. Dashed coordinates (——— ———) marked with "1 km," "2 km," and "1 day," refer to dimensional coordinates as described in Section V.F.1., p. 22. "Dimensional results" and coordinates in Figure 14 are described in Section V.F.1., p. 23.

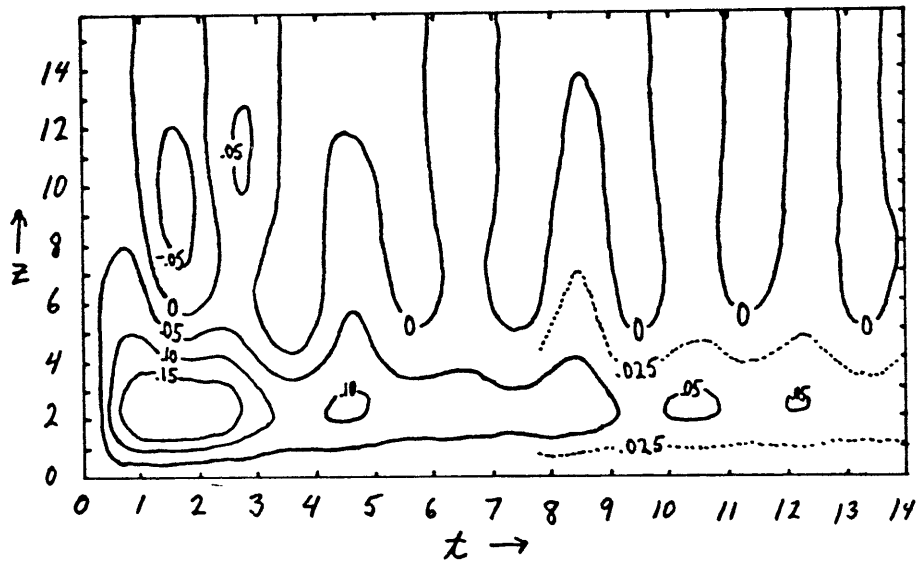

Figure 1. W Run 1, S = 0.4 , H = 15.8 See p. 26.

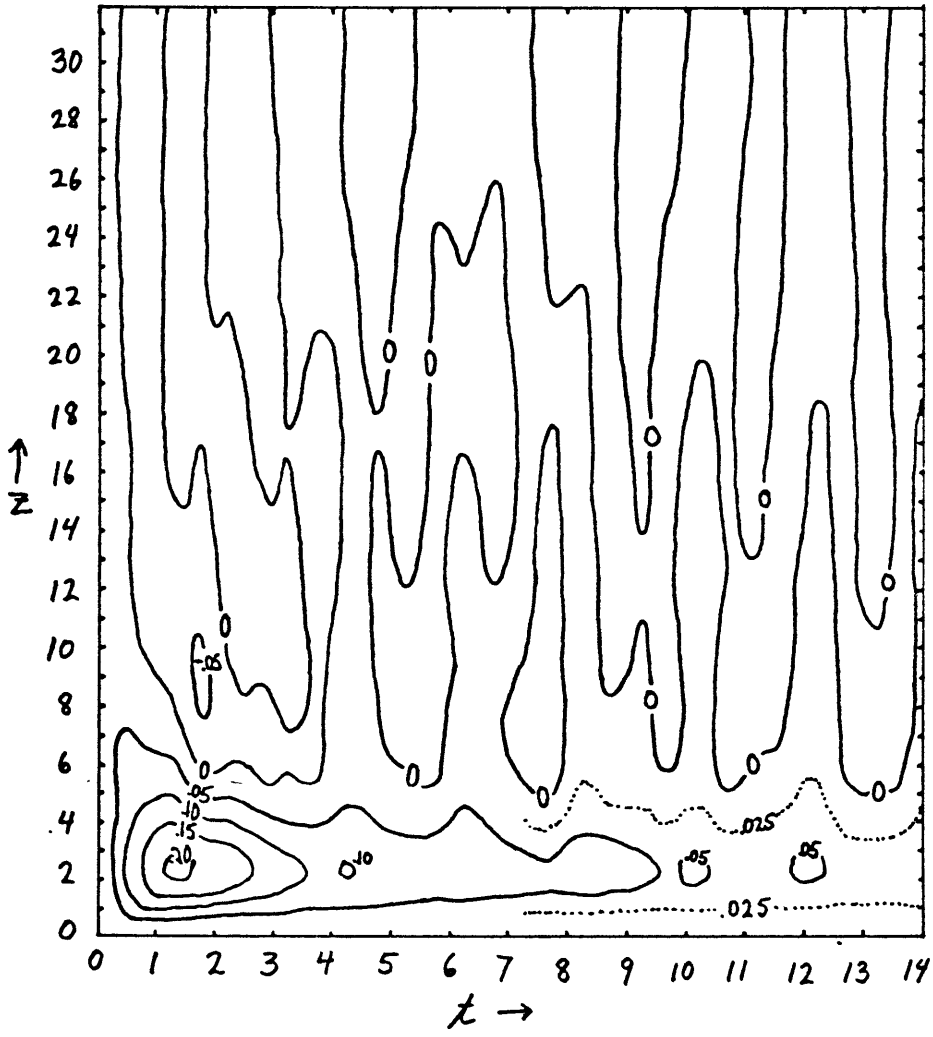

Figure 2. W Run 2, S = 0.4, H = 31.6 See p. 26.

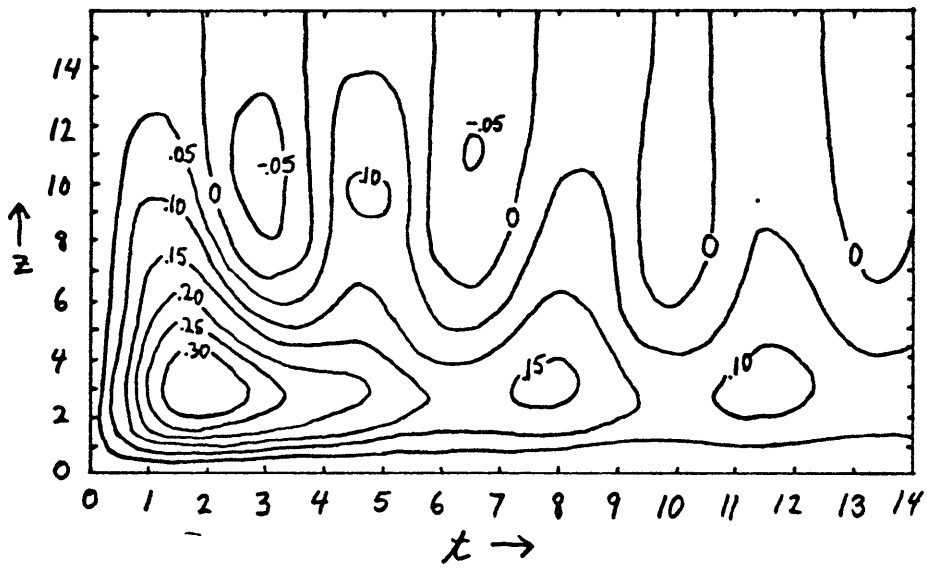

Figure 3. W Run 3, S = 0.1, H = 15.8 See p. 26.

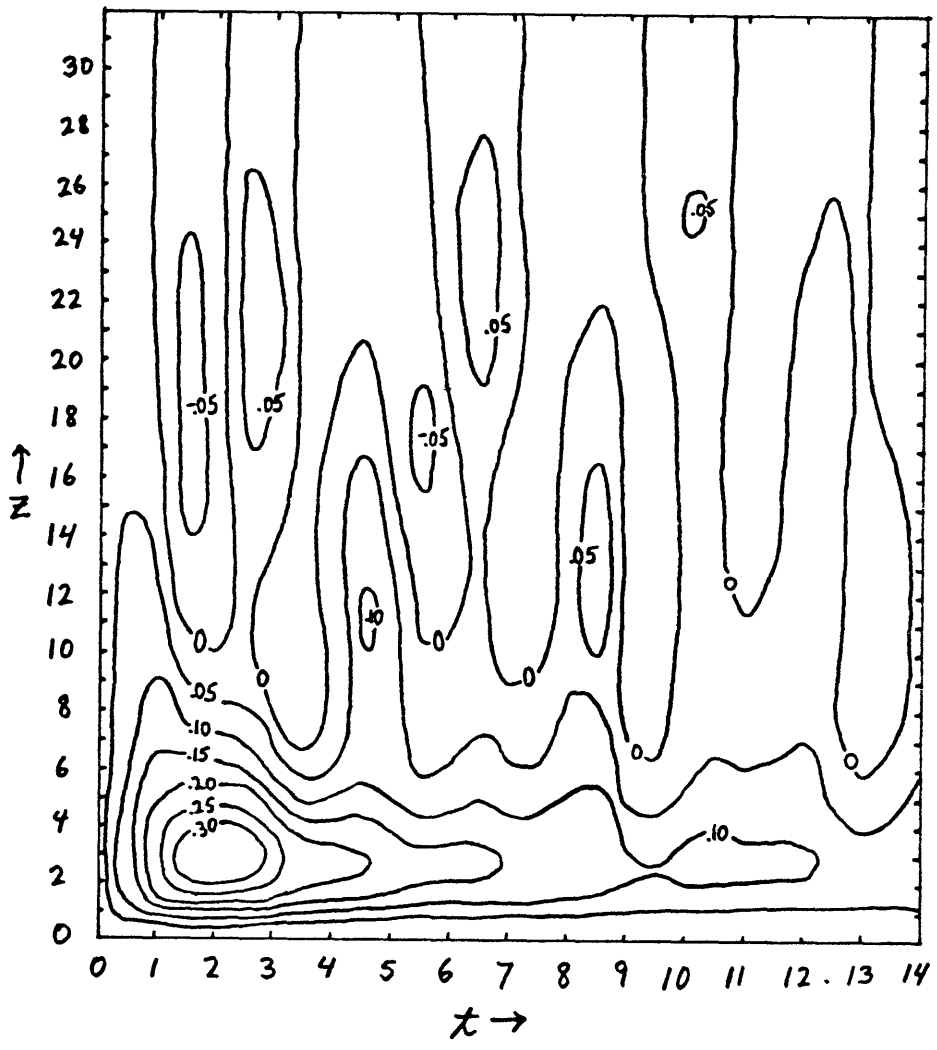

Figure 4. W Run 4, S = 0.1, H = 31.6 See p. 26.

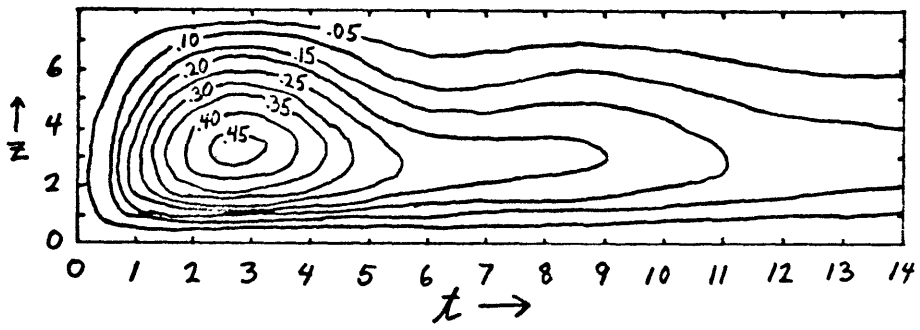

Figure 5. W Run 5, S = 0.01, H = 7.9 See p. 26

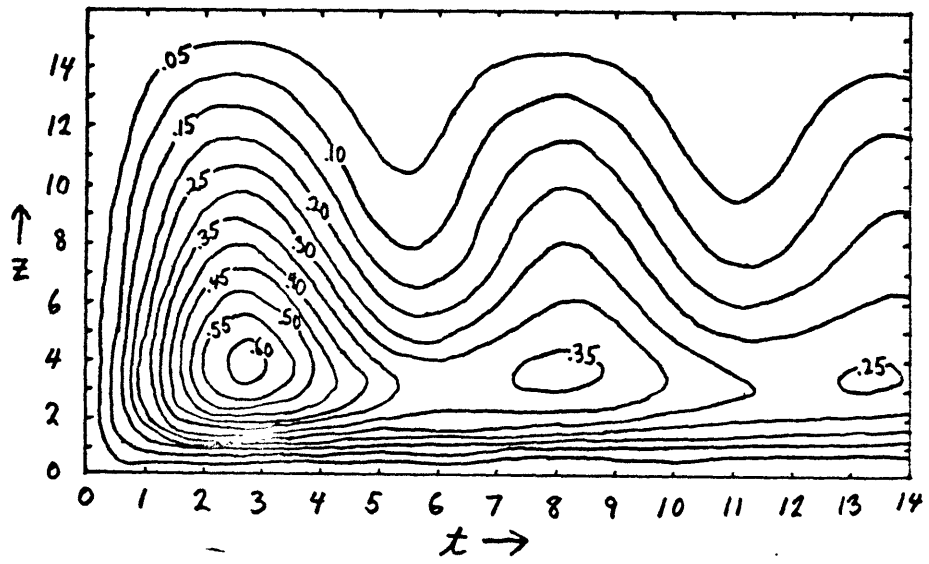

Figure 6. W Run 6, S = 0.01, H = 15.8 See p. 26.

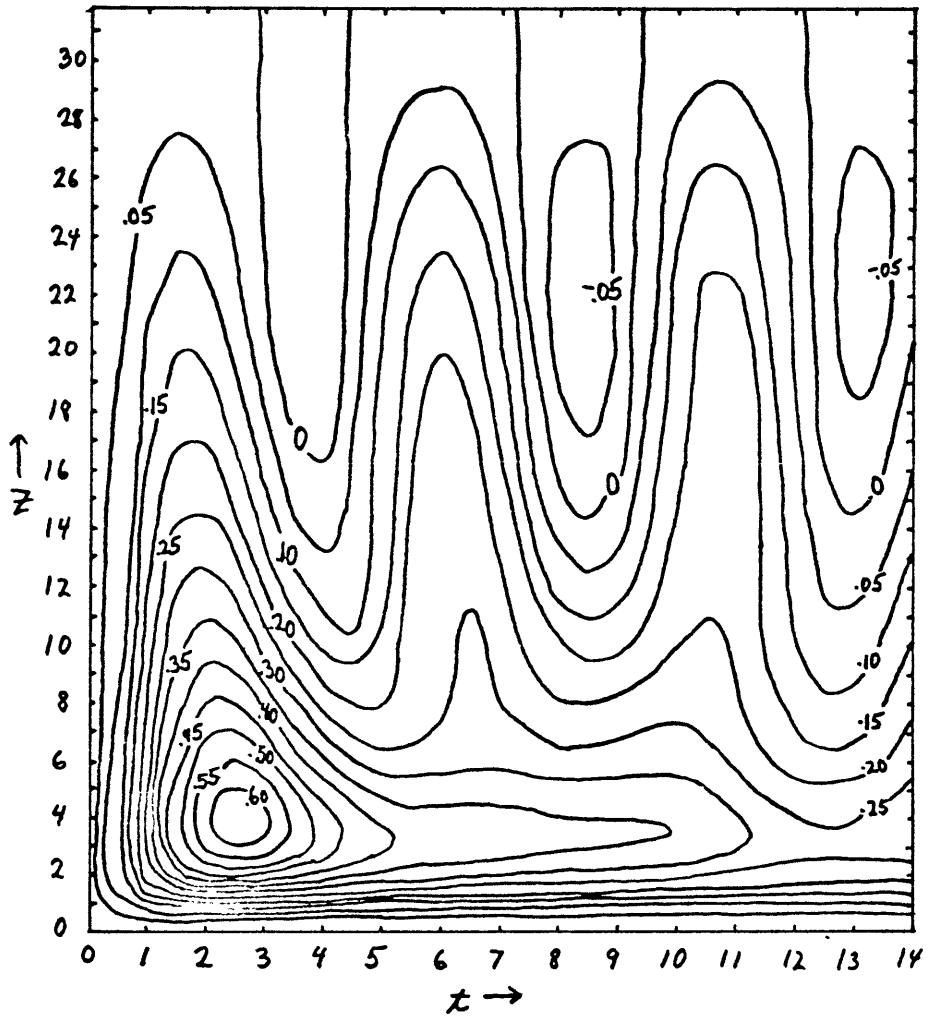

Figure 7. W Run 7, S = 0.01, H = 31.6 See p. 26.

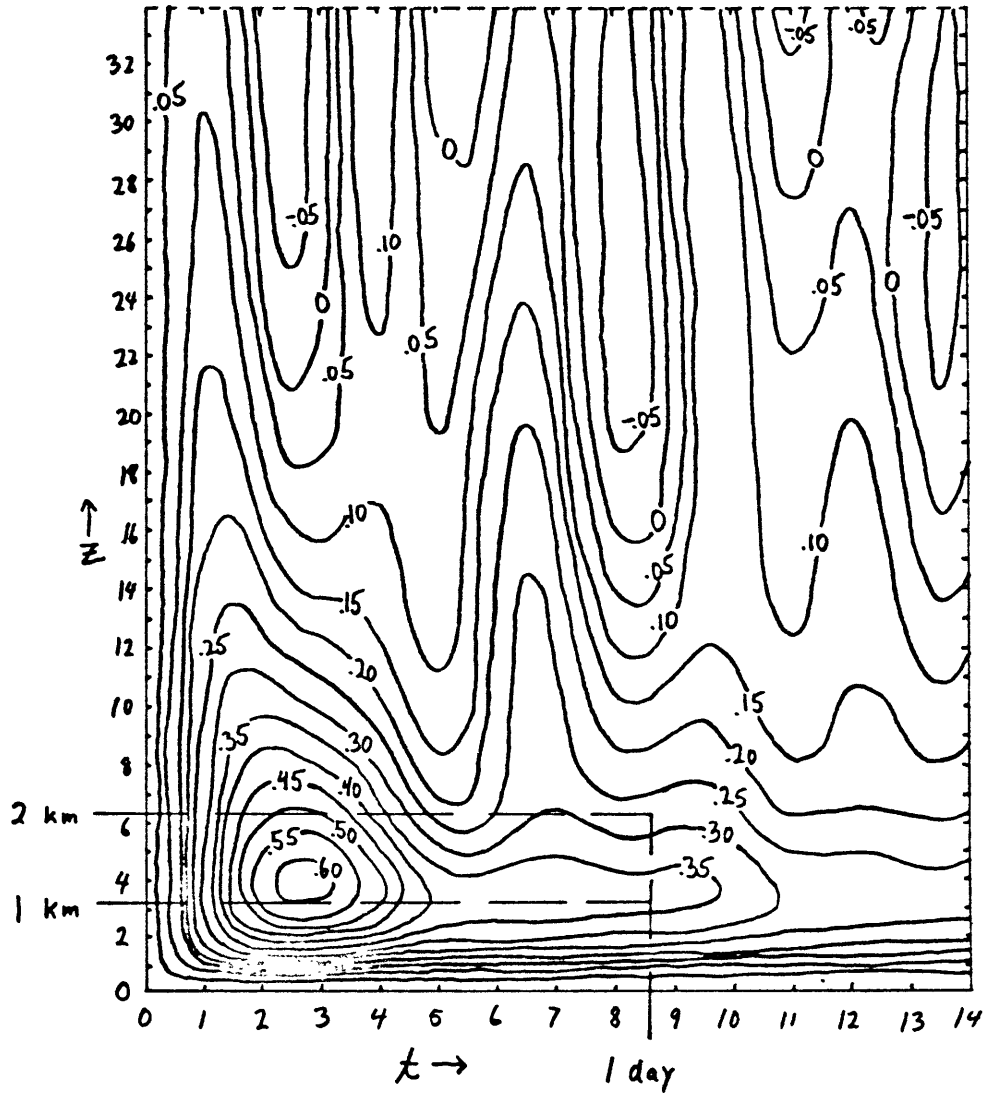

Figure 8. W Run 8, S = 0.01, H = 63.2 See p. 26.

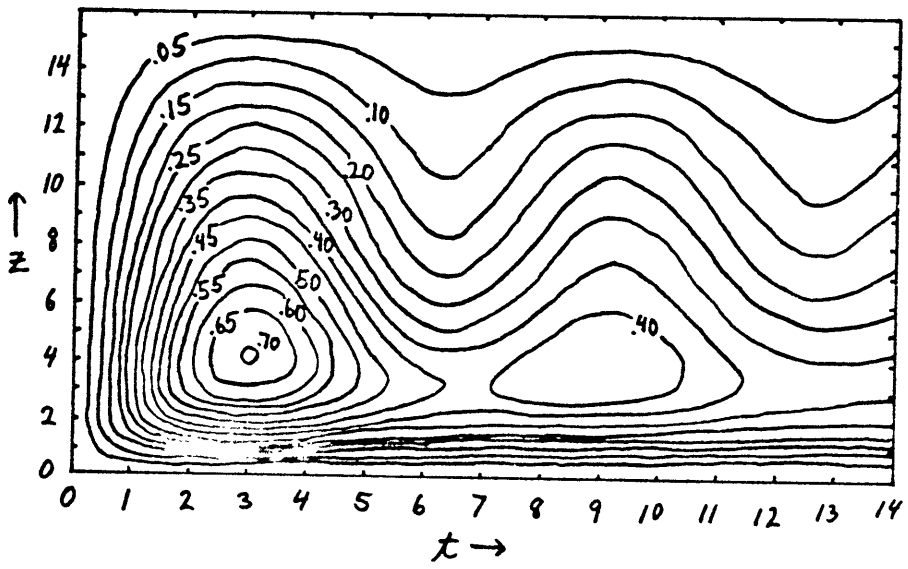

Figure 9. W Run 9, S = 0, H = 15.8 See p. 26.

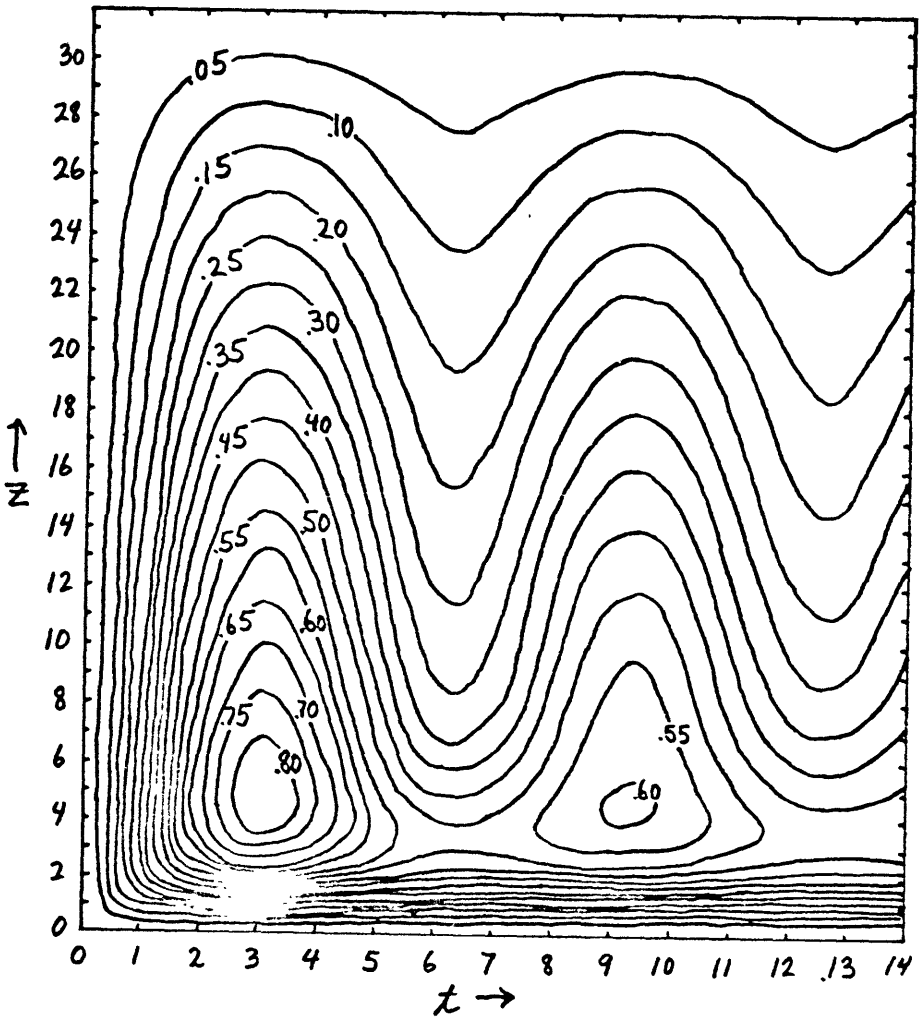

Figure 10. W Run 10, S = 0, H = 31.6 See p. 26.

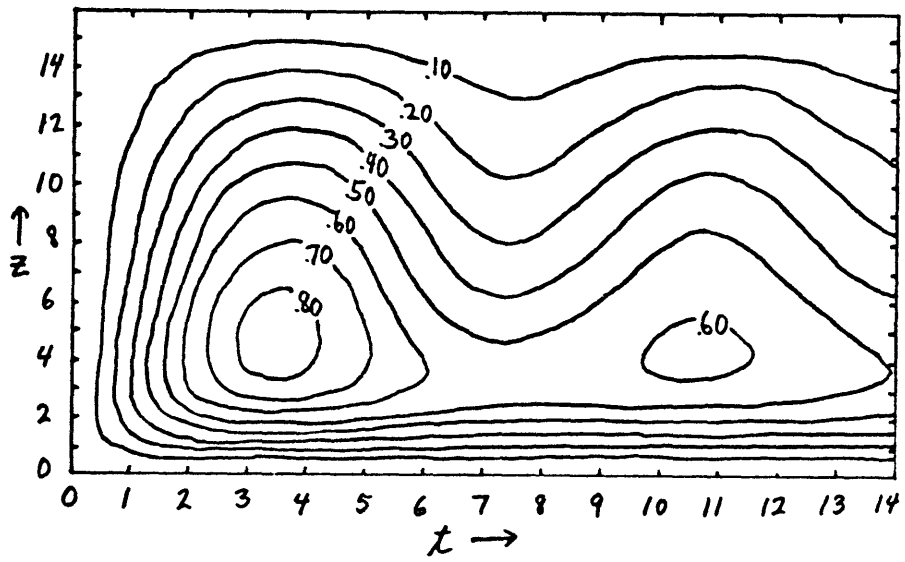

Figure 11. W Run 11, S = -0.01, H = 15.8 See p. 26.

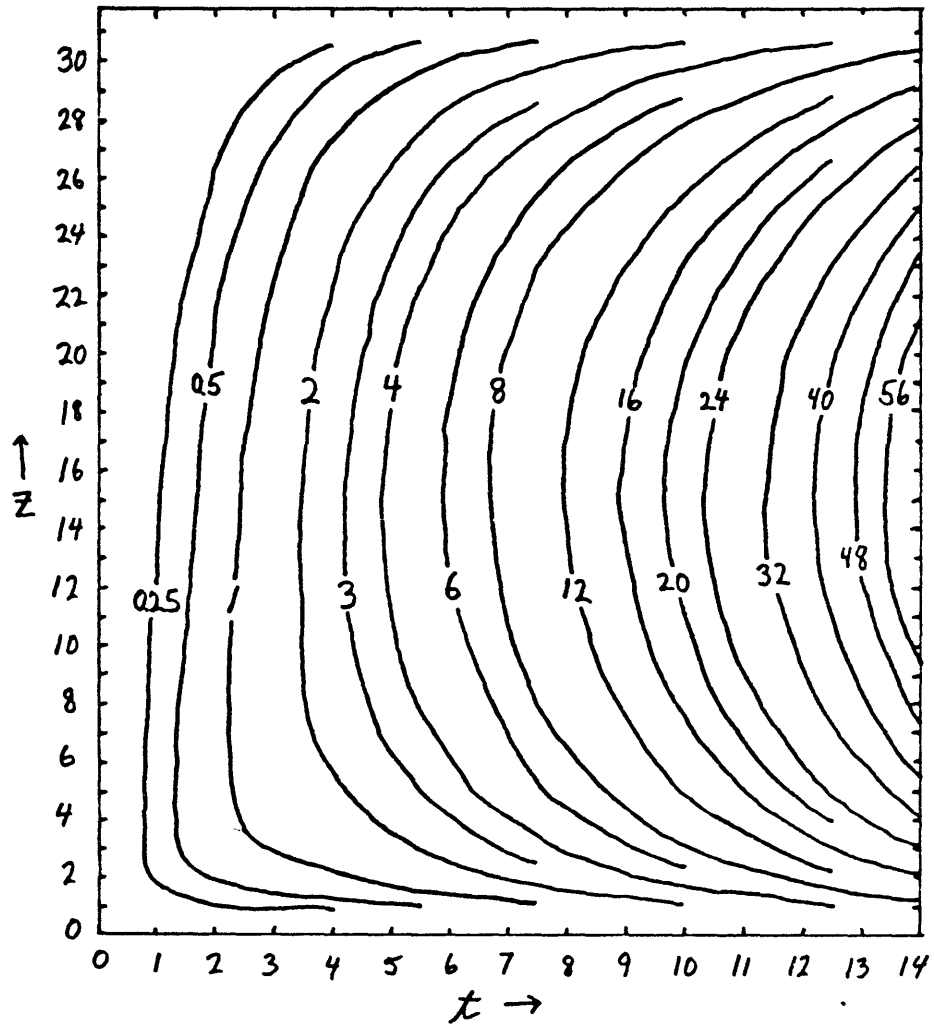

Figure 12. W Run 12, S = -0.01, H = 31.6 See p. 26.

TABLE 1 - LIST OF RUNS AND INERTIA-GRAVITY WAVES

Run	S	H	Theoretical				Observed	
			n=1		n=2		n=1	n=2
			Re ω	τ	Re ω	τ		
1	0.4	15.8	3.33	1.89	1.87	3.35	X	
2	0.4	31.6	6.44	0.98	3.33	1.89	X	X
3	0.1	15.8	1.87	3.35	1.28	4.91	X	
4	0.1	31.6	3.33	1.89	1.87	3.35	X	X
5	0.01	7.9	1.03	6.10	1.01	6.22	X	
6	0.01	15.8	1.12	5.60	1.03	6.10	X	
7	0.01	31.6	1.42	4.43	1.12	5.61	X	
8	0.01	63.2	2.25	2.80	1.42	4.43	X	
9	0	15.8	1.00	6.28	1.00	6.28	X	
10	0	31.6	1.00	6.28	1.00	6.28	X	
11	-0.01	15.8	0.86	7.32	0.97	6.48	X	
12	-0.01	31.6	Im	Im	0.86	7.32		
13	0.16	63.2	8.12	0.77	4.15	1.51	X	X
14	2.56	63.2	32.21	0.20	16.15	0.39	X	X
15	0.01	63.2	2.25	2.80	1.42	4.43	X	

Run 15 started with an Ekman-quasi-geostrophic profile.

Re ω = frequency of inertia-gravity waves

τ = period of inertia-gravity waves

TABLE 2 - WMAX

Run	S	H	a	b	c	d
1	0.4	15.8	2.3	2.3	1.5	0.20
2	0.4	31.6	2.5	2.3	1.4	0.21
3	0.1	15.8	2.9	2.7	2.0	0.35
4	0.1	15.8	2.9	2.6	2.0	0.35
5	0.01	7.9	3.33	2.9	2.5	0.46
6	0.01	15.8	3.7	3.3	2.8	0.61
7	0.01	31.6	3.9	3.4	2.5	0.63
8	0.01	63.2	3.8	3.4	2.5	0.62
9	0	15.8	4.2	3.5	3.0	0.70
10	0	31.6	4.8	4.0	3.0	0.84
11	-0.01	15.8	4.7	3.9	3.5	0.85
12	-0.01	31.6	---	---	---	----
13	0.16	63.2	2.7	2.6	1.8	0.30
14	2.56	63.2	1.8	1.7	0.8	0.09

a $\approx$ z (first Wmax)

b $\approx \overline{z}$ (Wmax after first peak)

c $\approx$ t (initial Wmax)

d $\approx$ initial Wmax

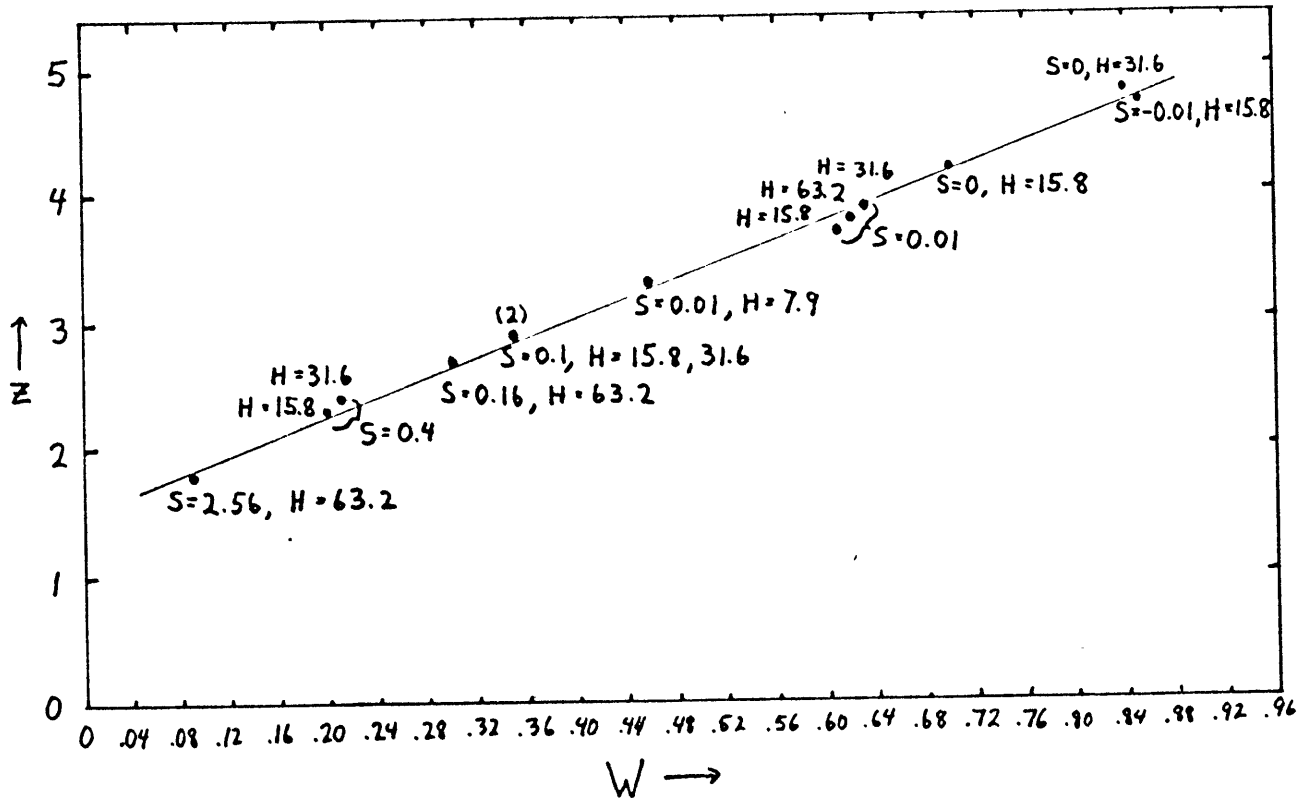

Figure 13. First Wmax vs. z(first W max)

See p. 26.

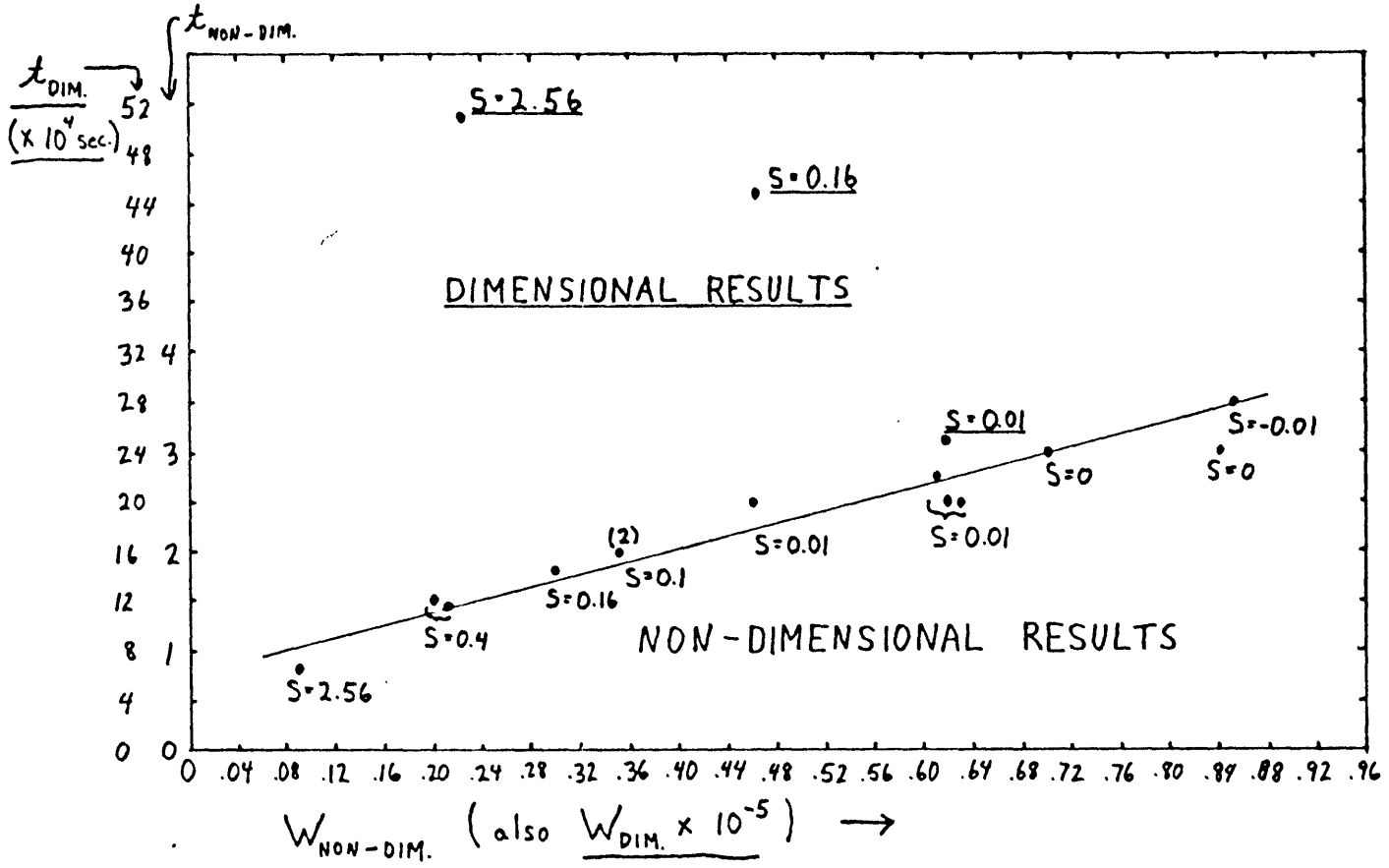

Figure 14. First Wmax vs. t(first Wmax)

See p. 26.

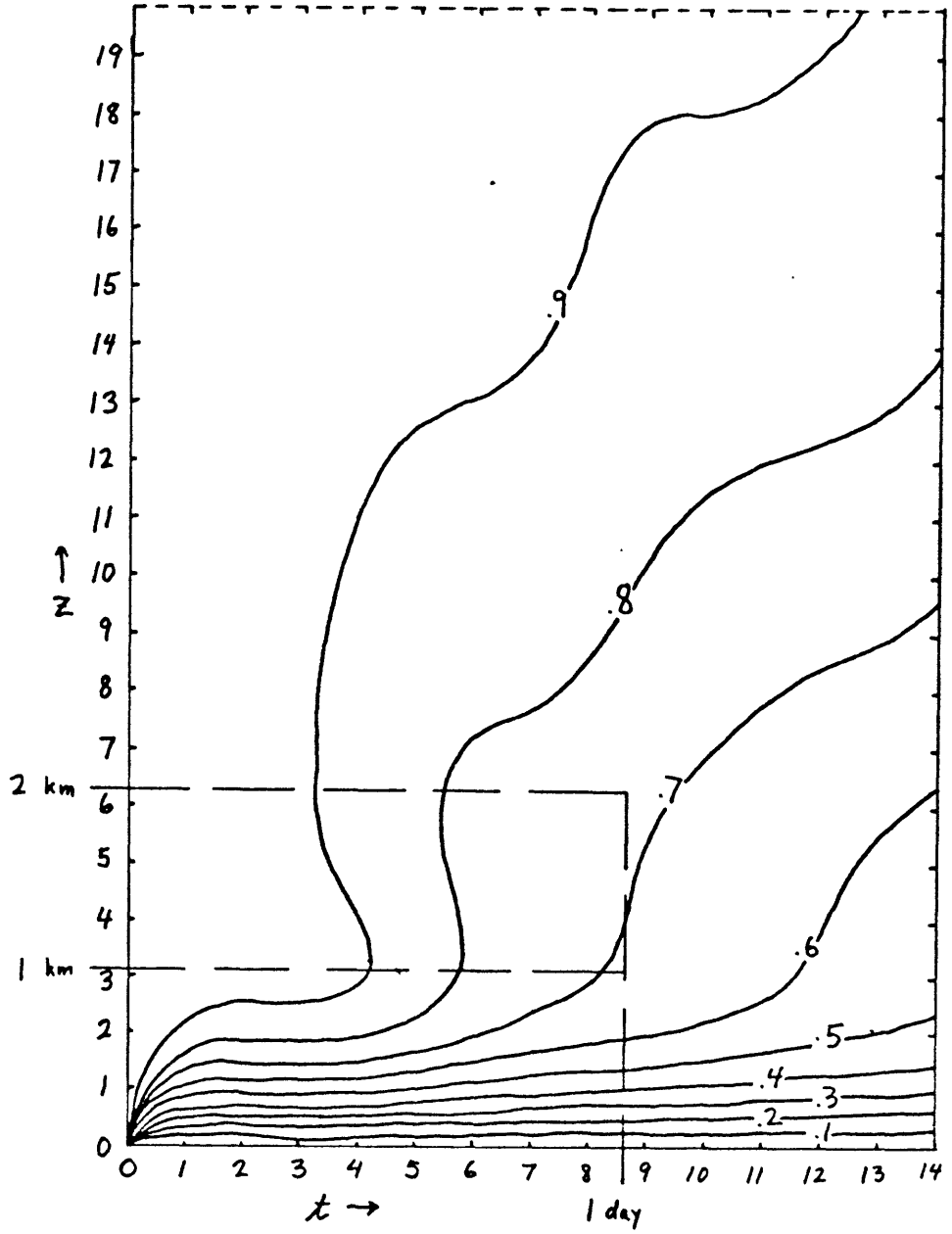

Figure 15. V Run 8, S = 0.01, H = 63.2 See p. 26.

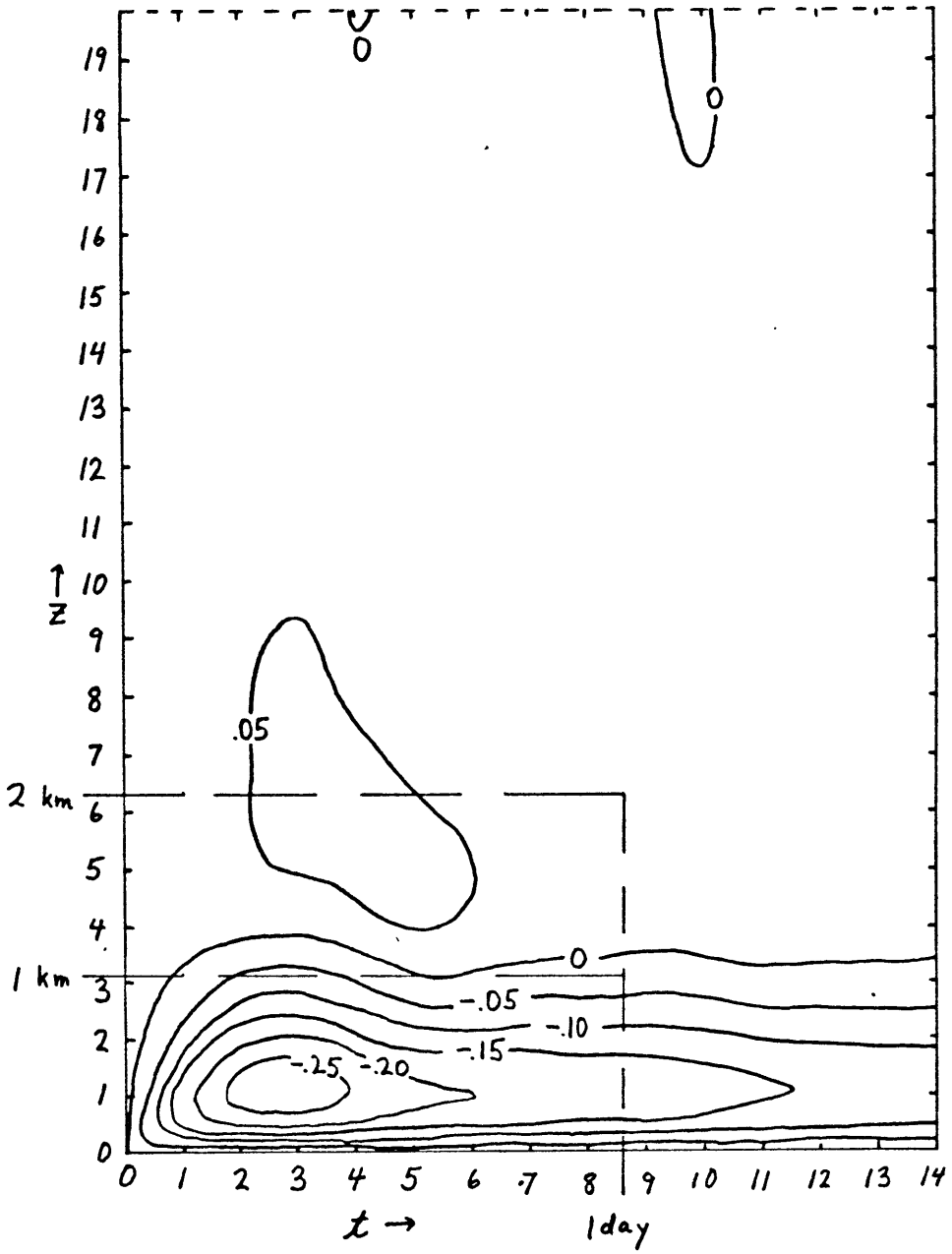

Figure 16. U Run 8, S = 0.01, H = 63.2 See p. 26.

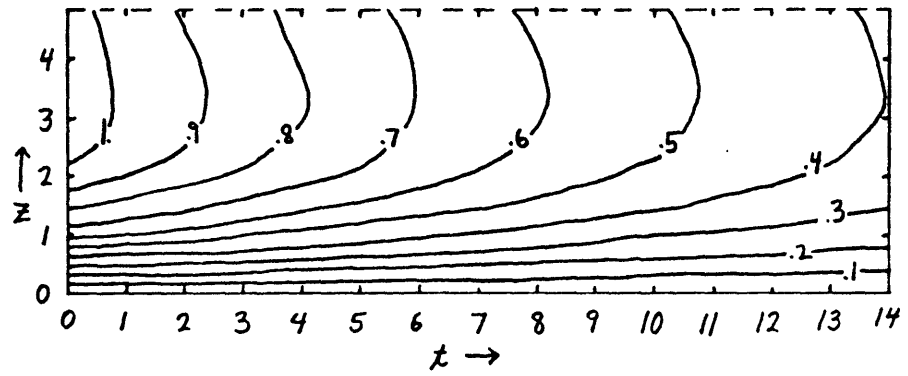

Figure 17. VEK Run 8, S = 0.01, H = 63.2 See p. 26.

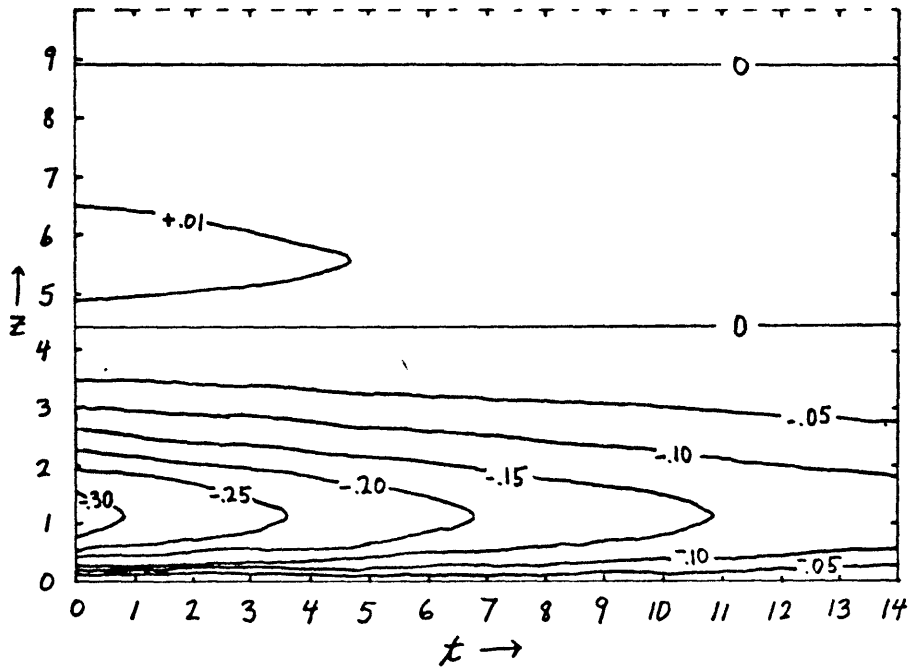

Figure 18. UEK Run 8, S = 0.01, H = 63.2 See p. 26.

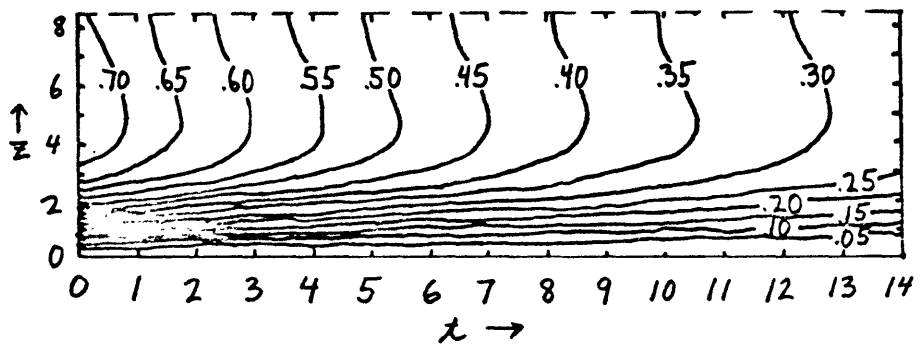

Figure 19. WEK Run 8, S = 0.01, H = 63.2 See p. 26.

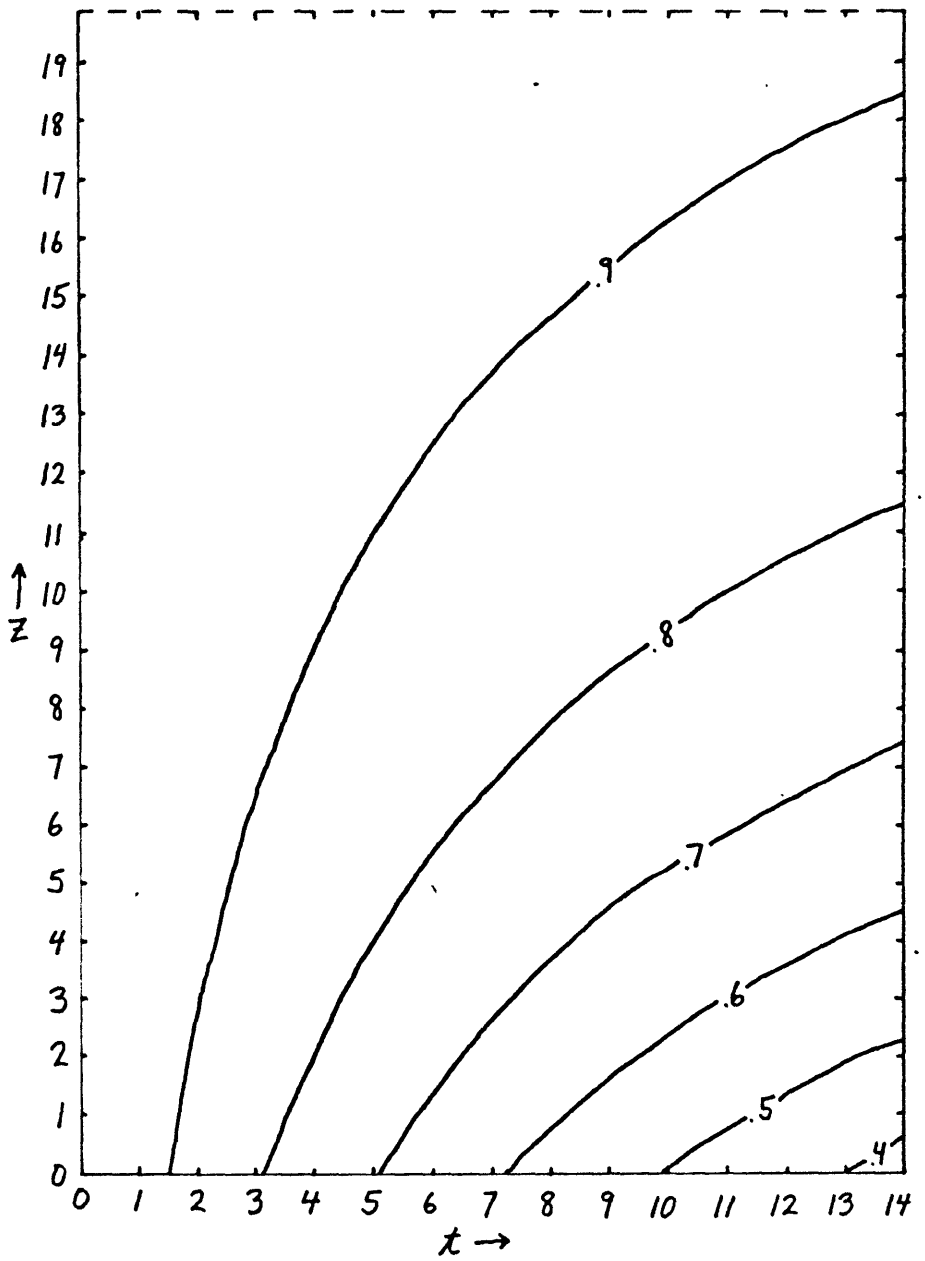

Figure 20. VQG Run 8, S = 0.01, H = 63.2 See p. 26.

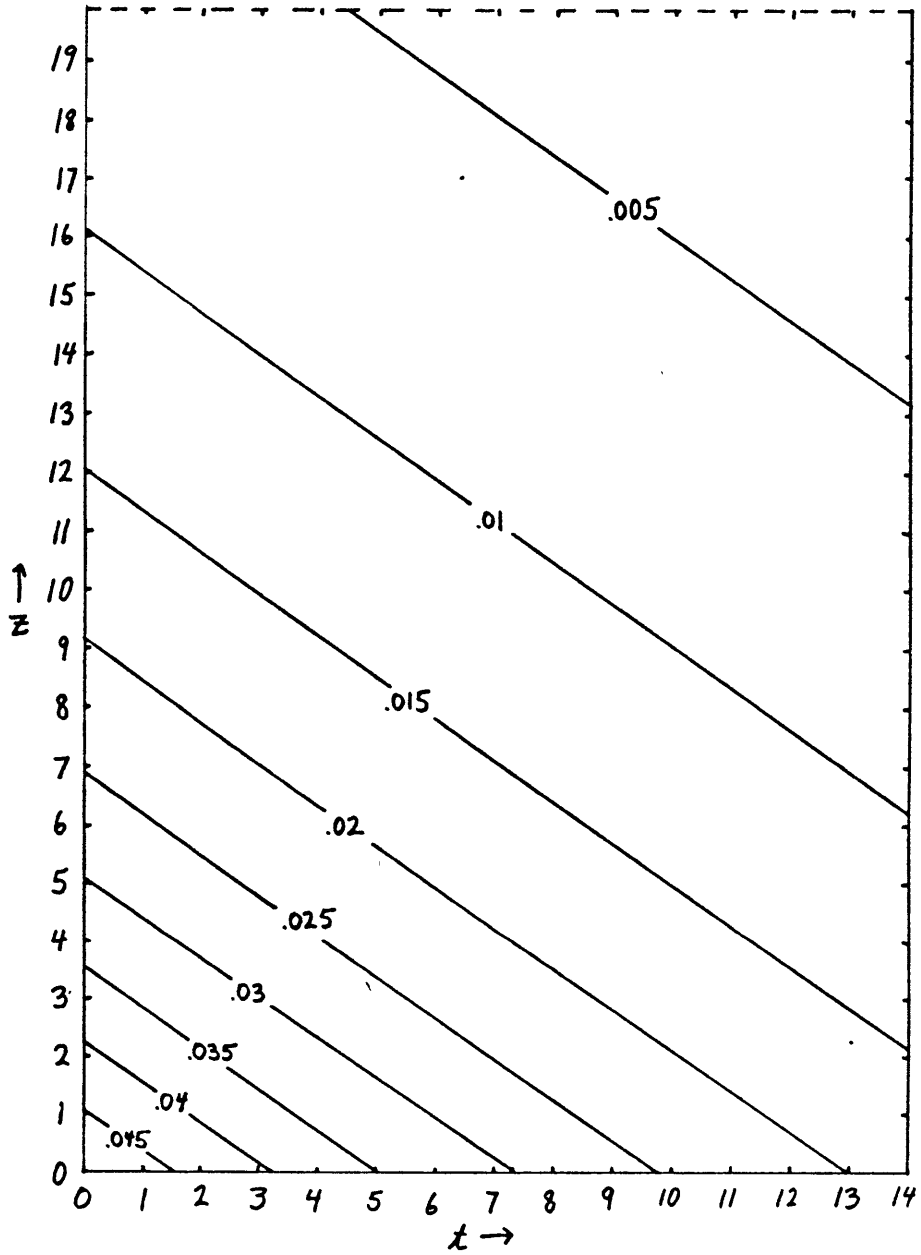

Figure 21. UQG Run 8, S = 0.01, H = 63.2 See p. 26.

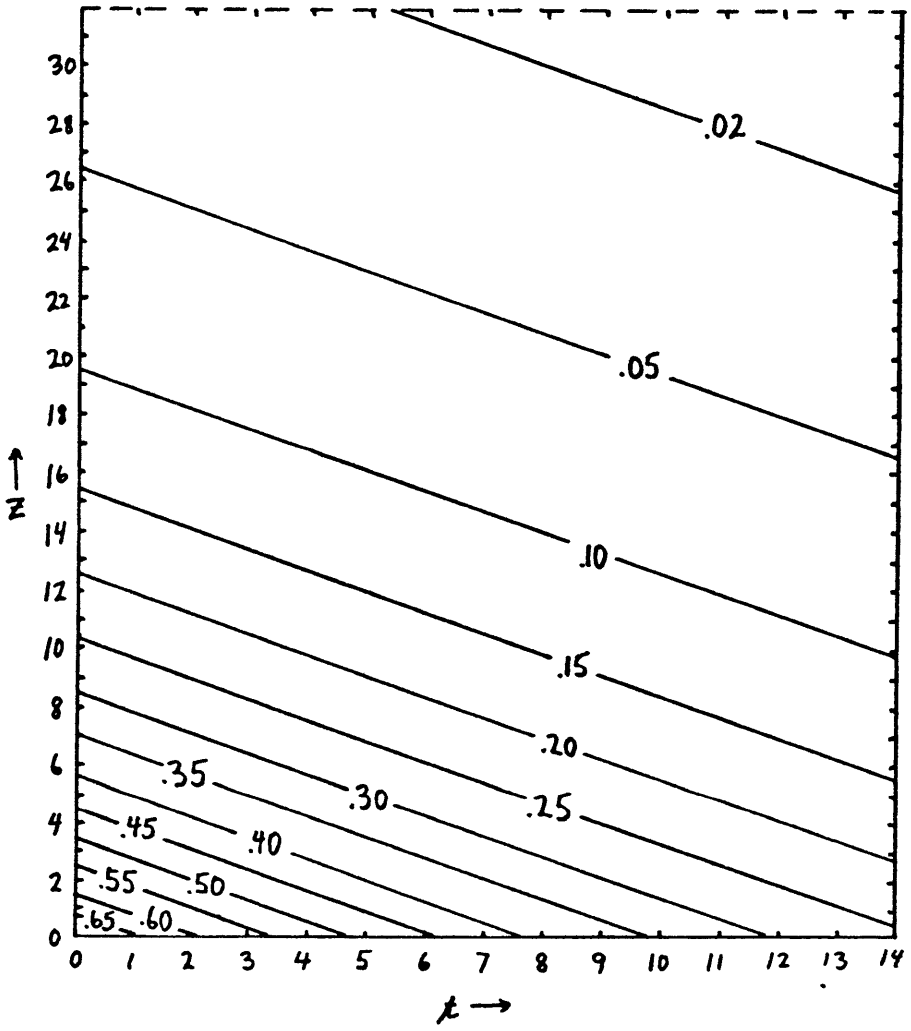

Figure 22. WQG Run 8, S = 0.01, H = 63.2 See p. 26.

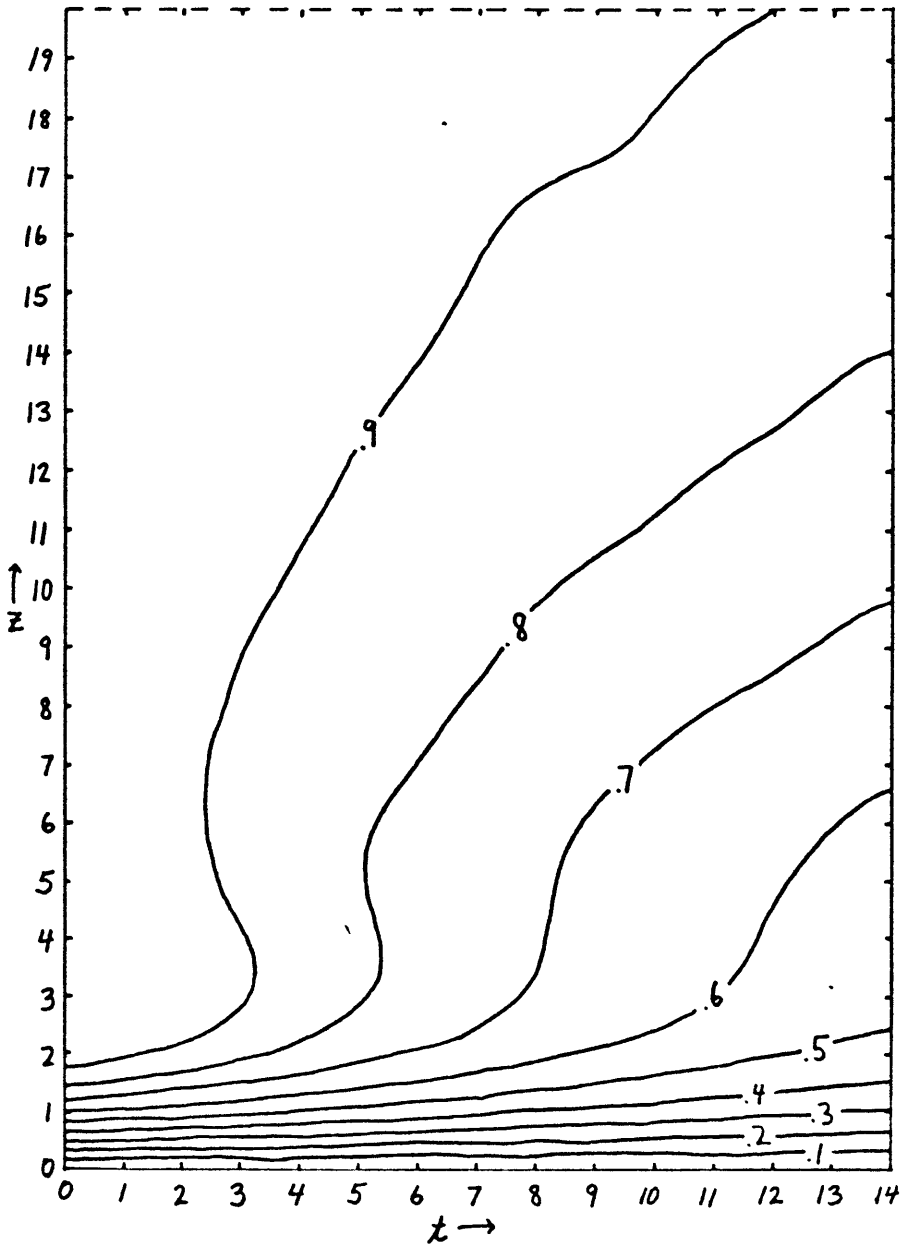

Figure 23. V Run 15, S = 0.01, H = 63.2 See p. 26.

EK-QG Start

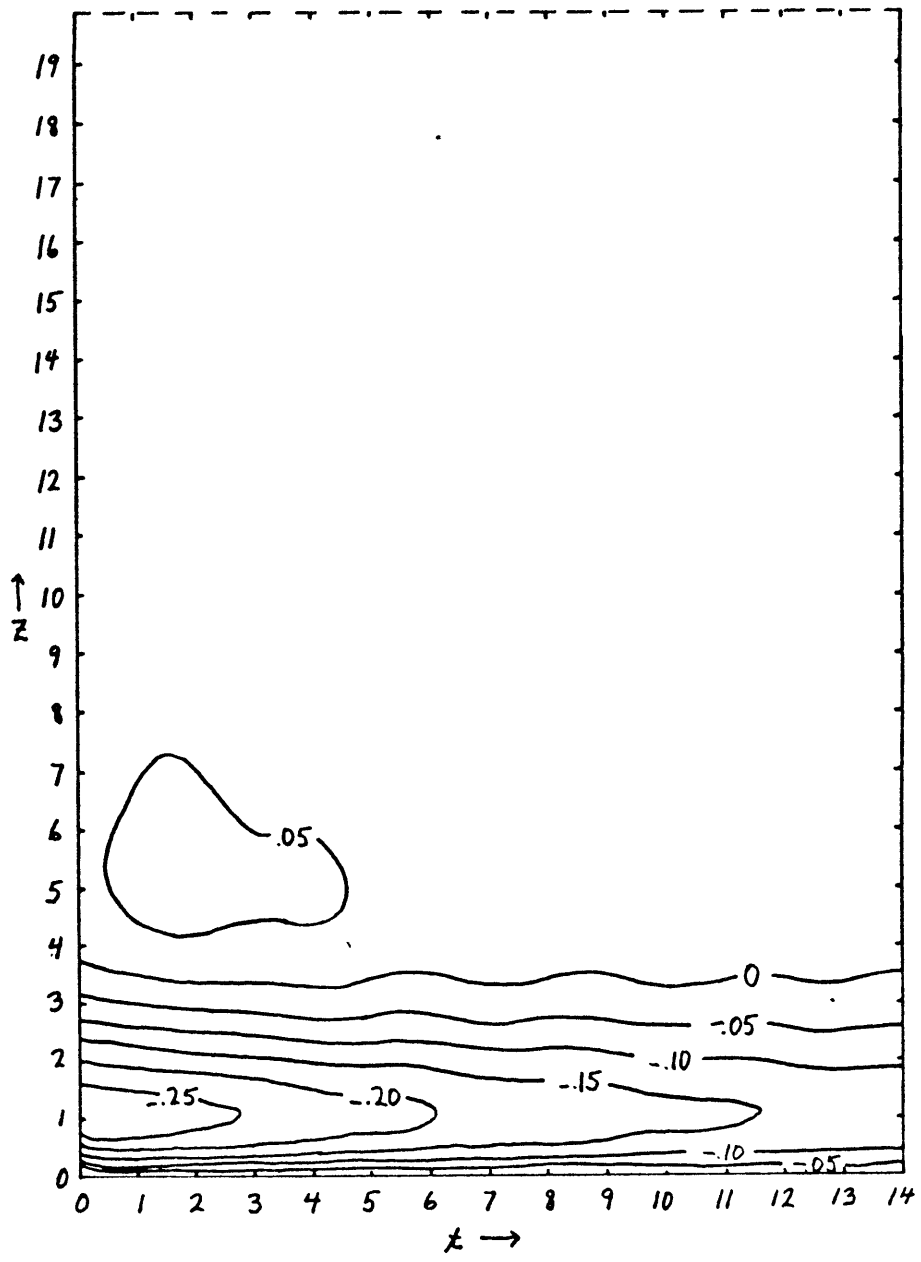

Figure 24. U Run 15, S = 0.01, H = 63.2 See p. 26.

EK-QG Start

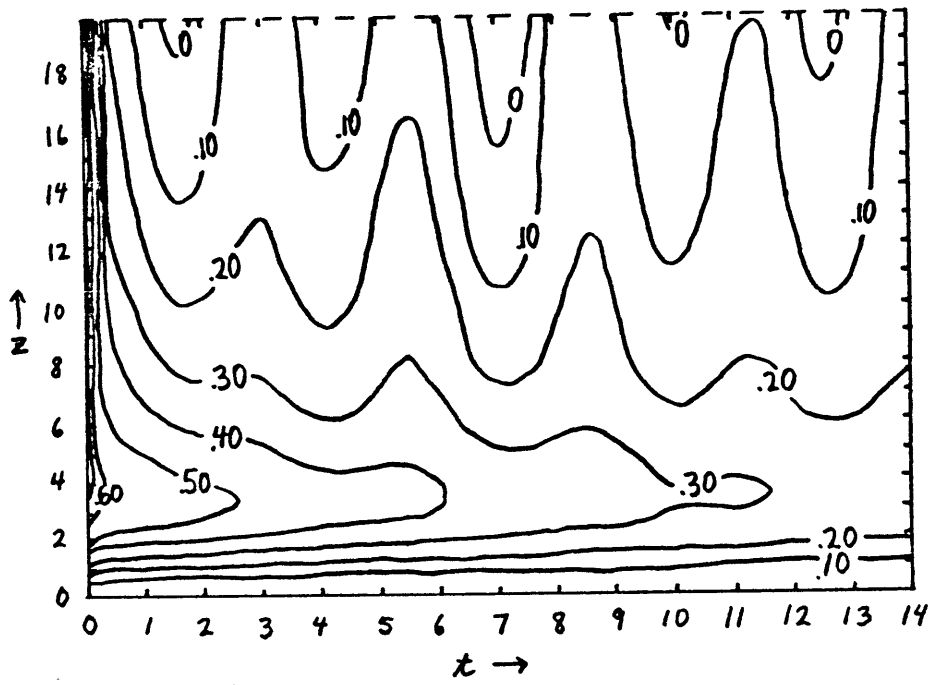

Figure 25. W Run 15, S = 0.01, H = 63.2 See p. 26.

EK-QG Start

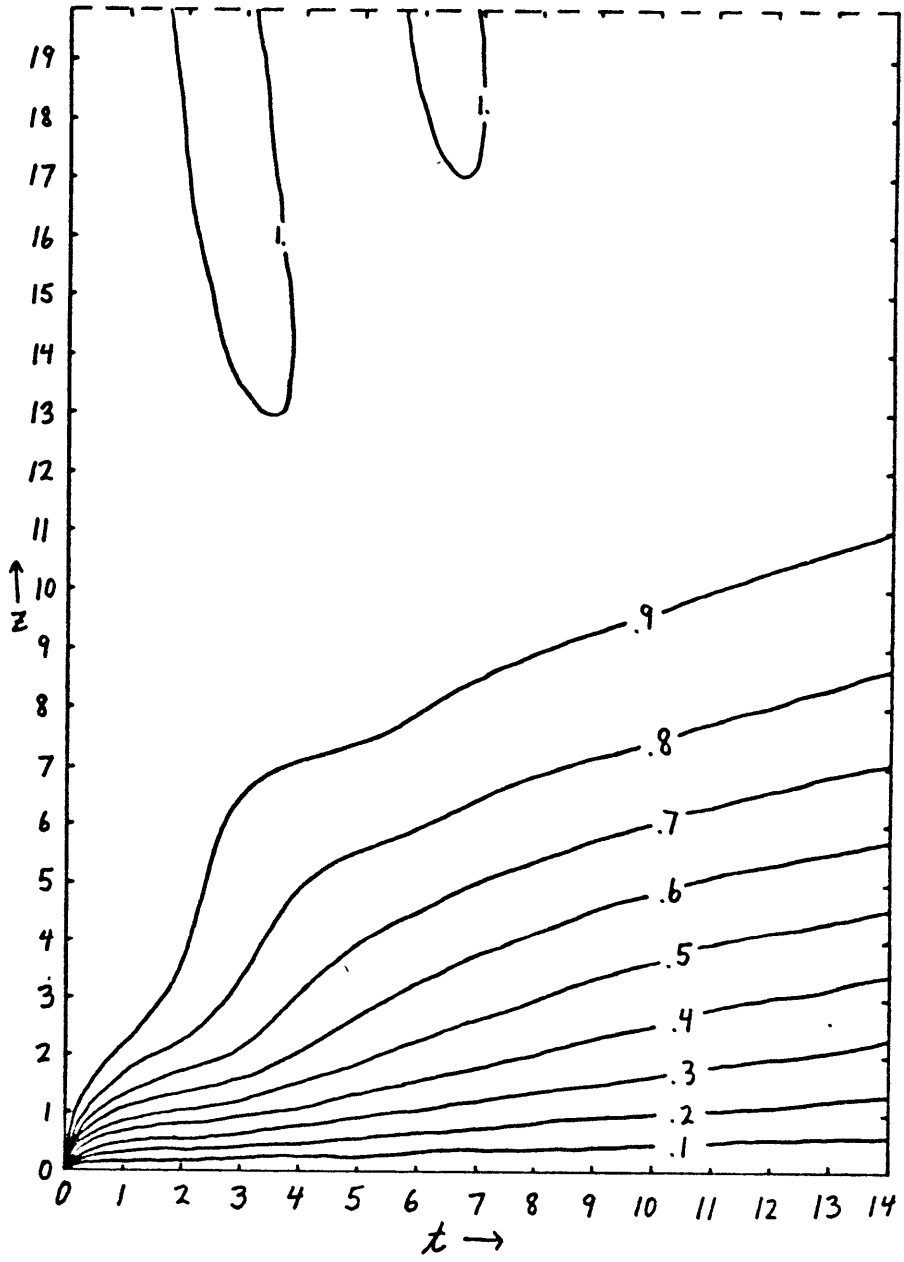

Figure 26. V Run 13, S = 0.16, H = 63.2 See p. 26.

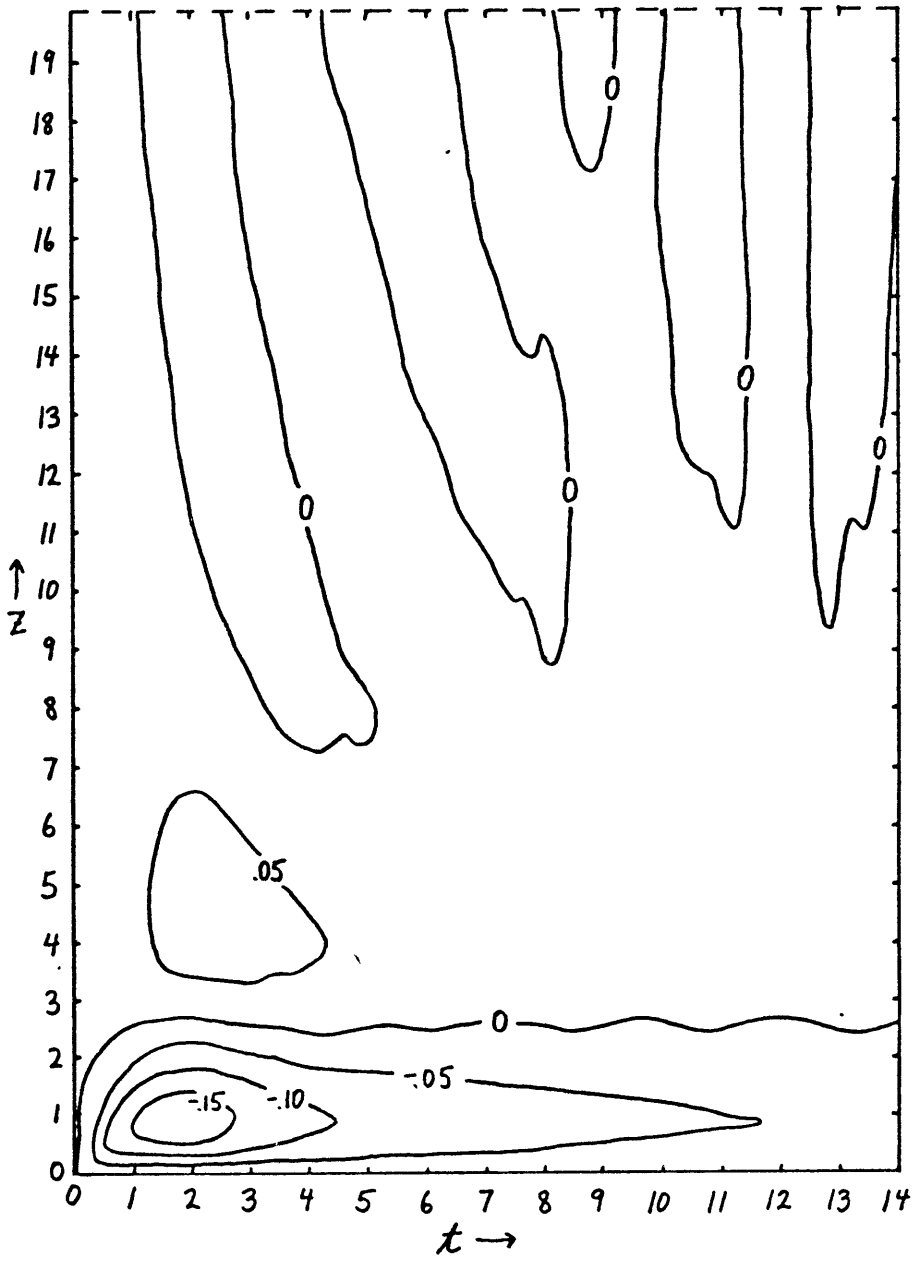

Figure 27. U Run 13, S = 0.16, H = 63.2 See p. 26.

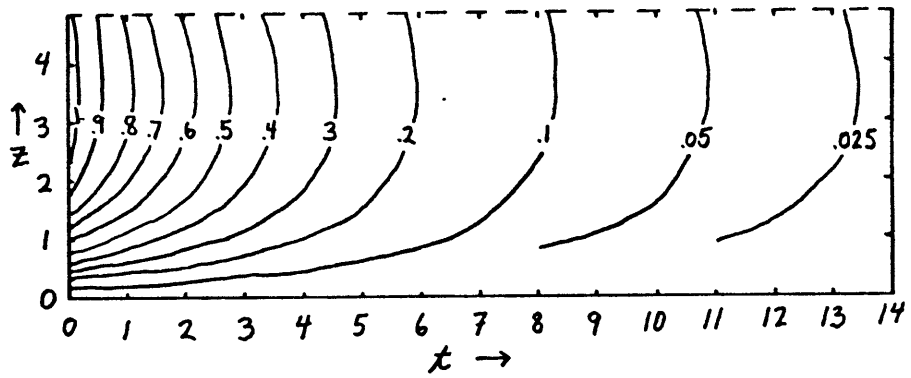

Figure 28. VEK Run 13, S = 0.16, H = 63.2 See p. 26.

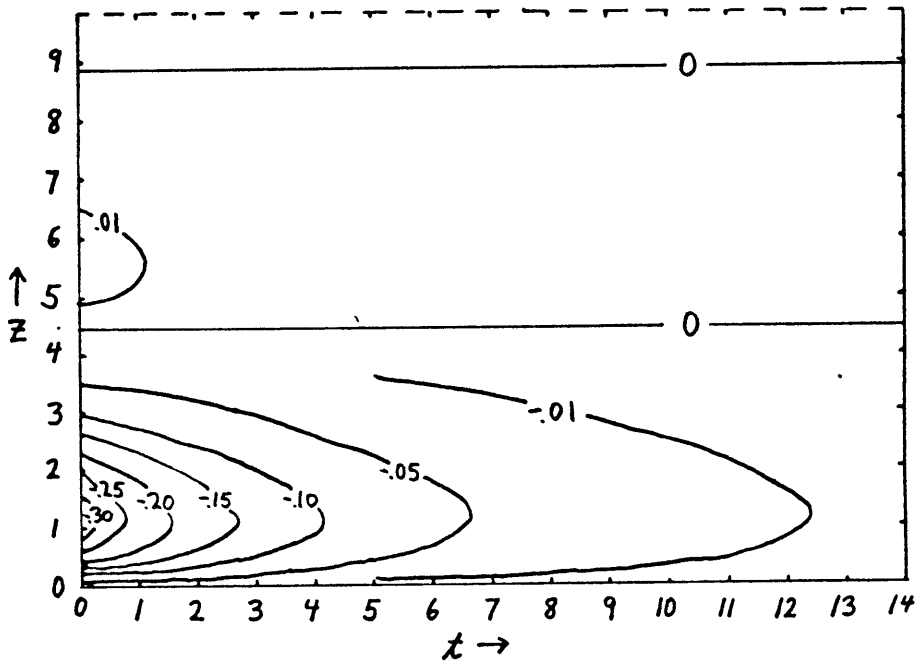

Figure 29. UEK Run 13, S = 0.16, H = 63.2 See p. 26.

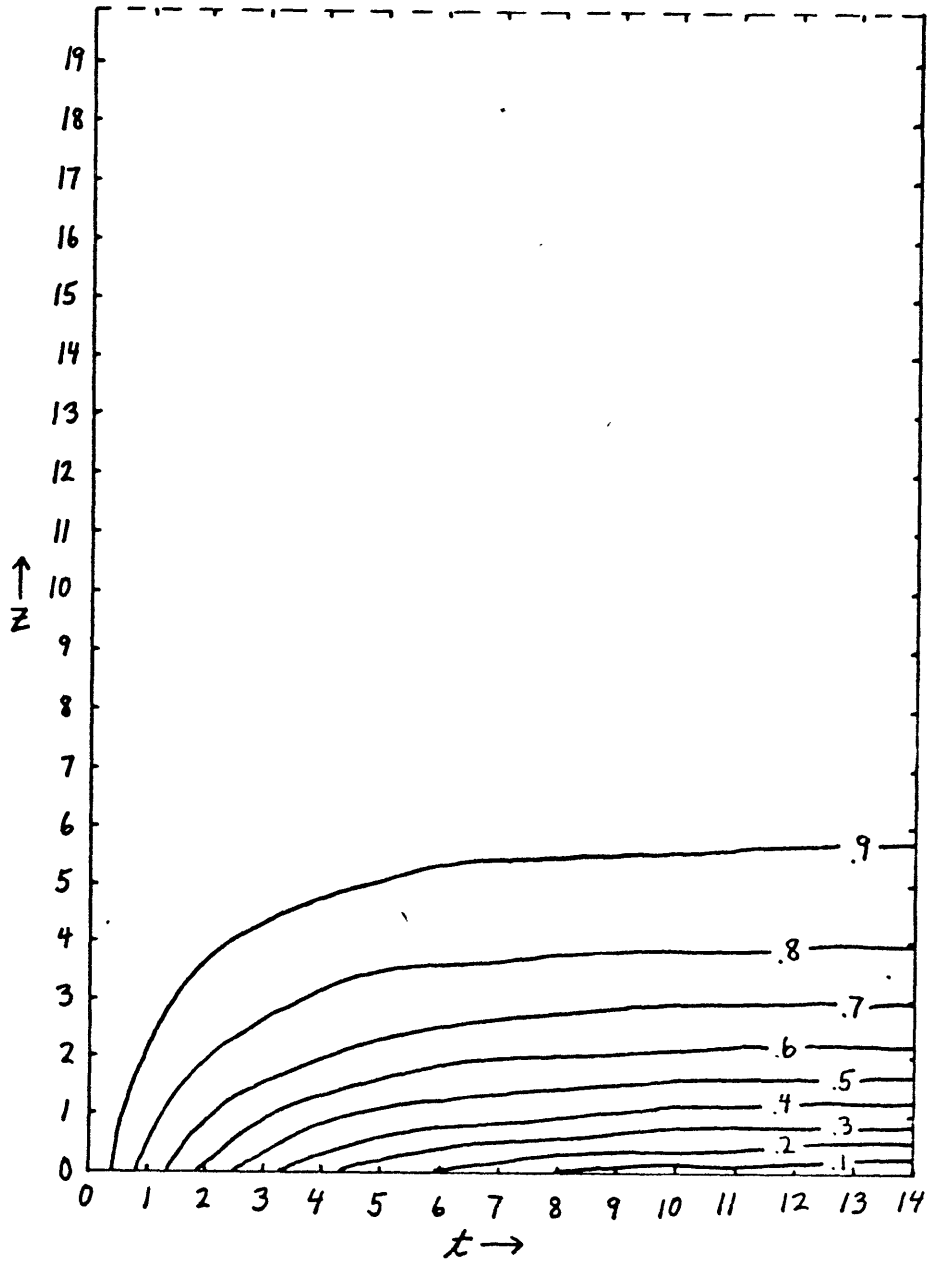

Figure 30. VQG Run 13, S = 0.16, H = 63.2 See p. 26.

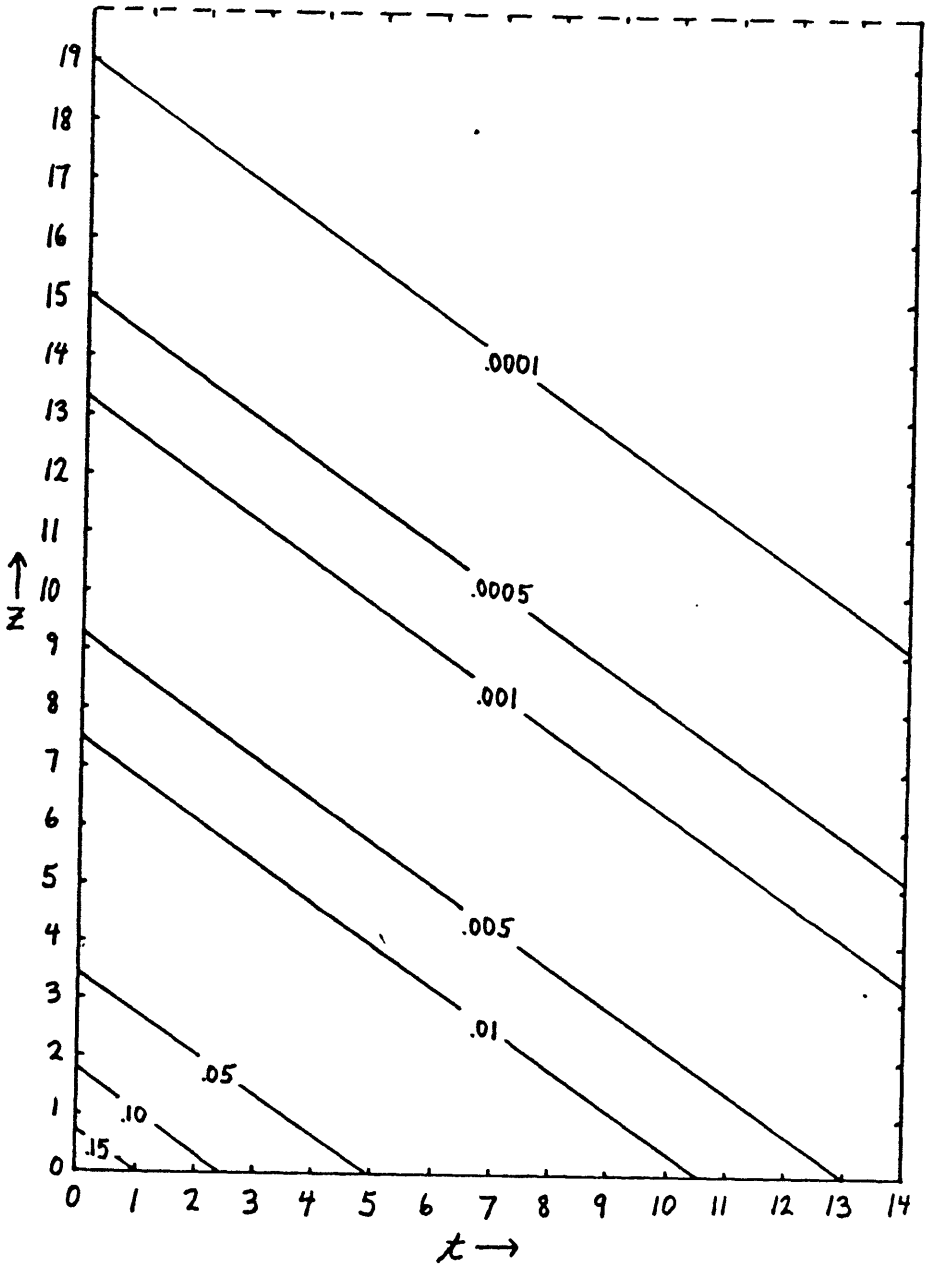

Figure 31. UQG Run 13, S = 0.16, H = 63.2 See p. 26.

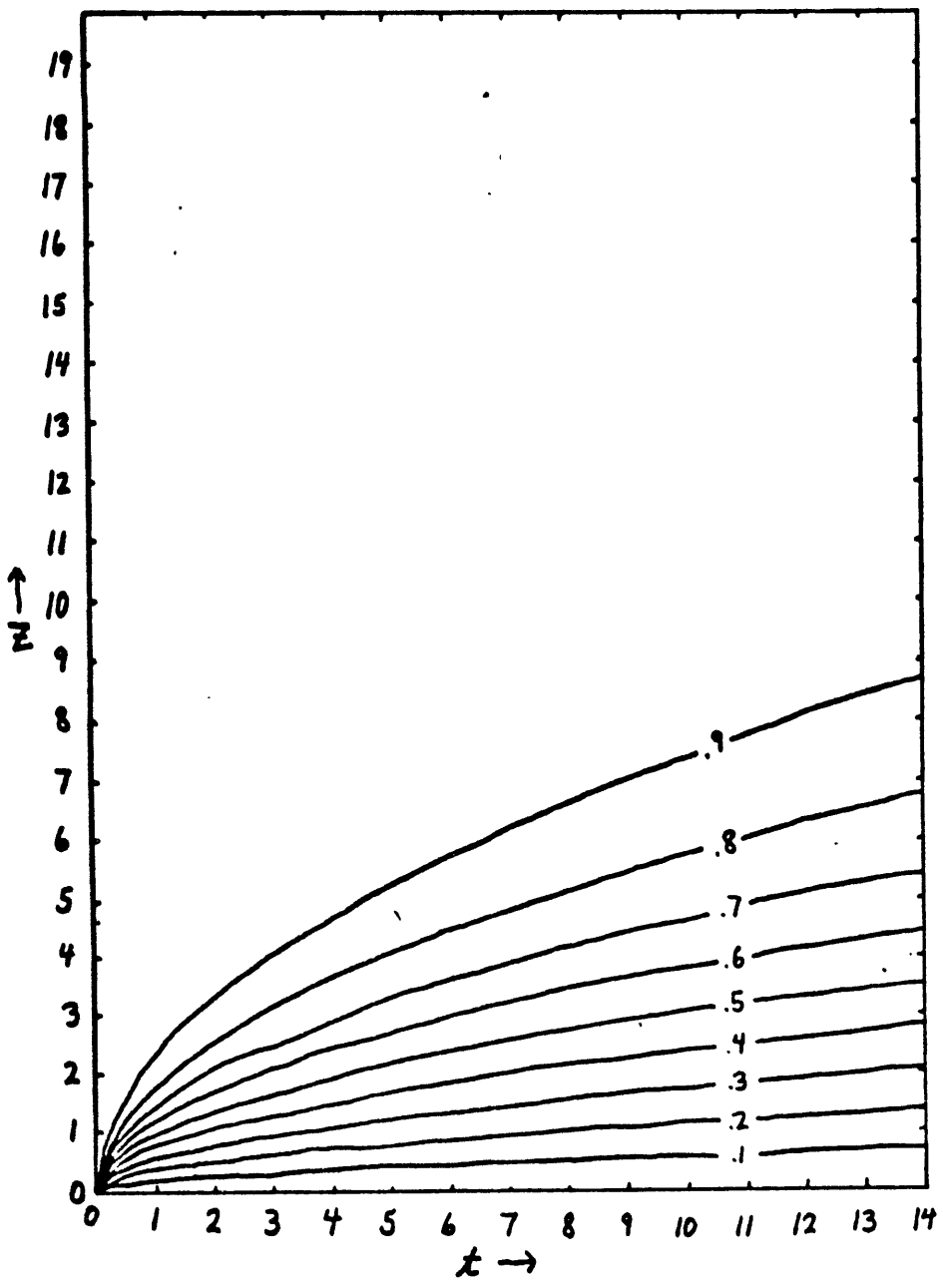

Figure 32. Pure diffusion solution, $V = \mathrm{erf}(z/2\sqrt{t})$

See p. 26.

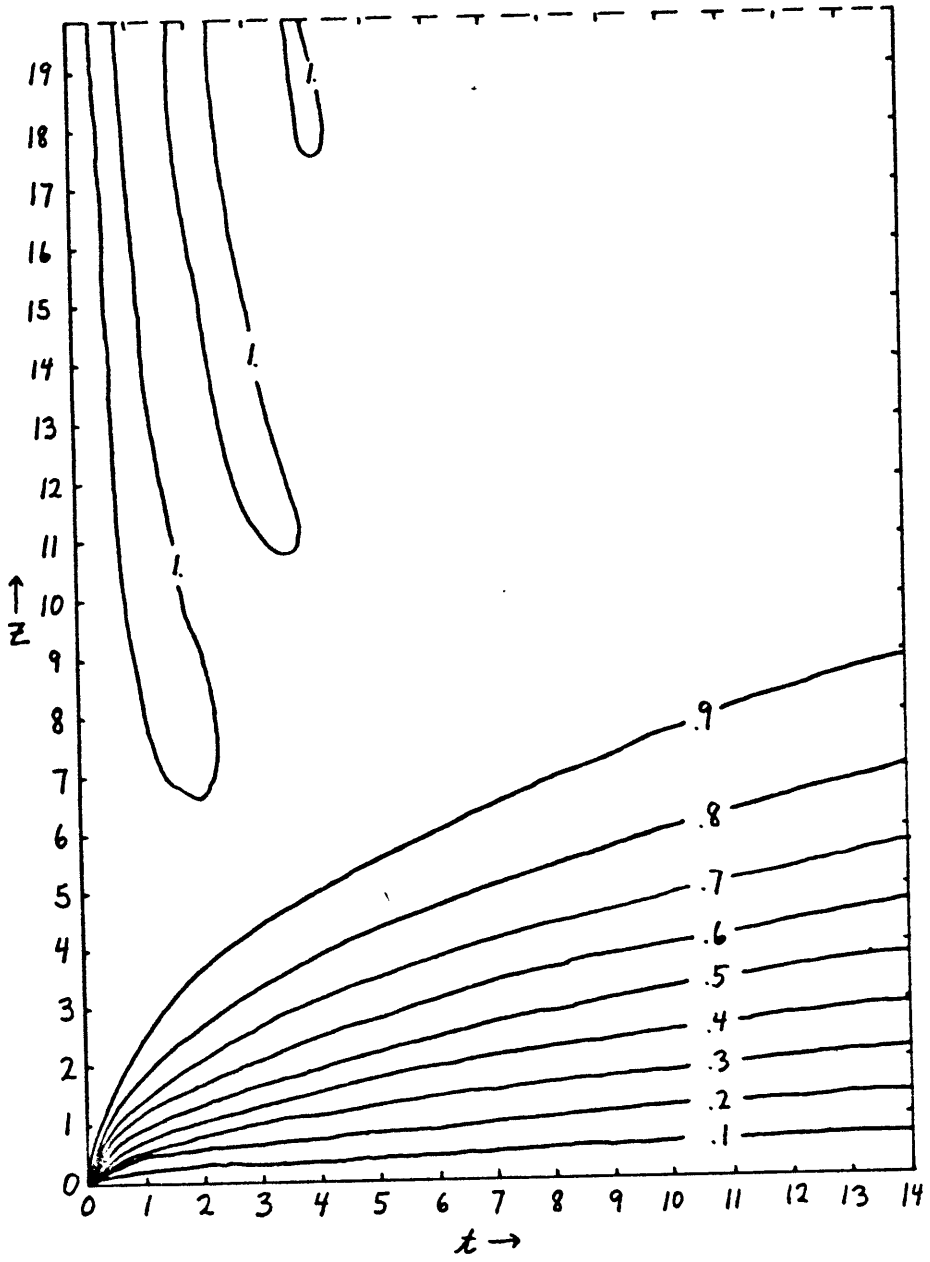

Figure 33. V Run 14, S = 2.56, H = 63.2 See p. 26.

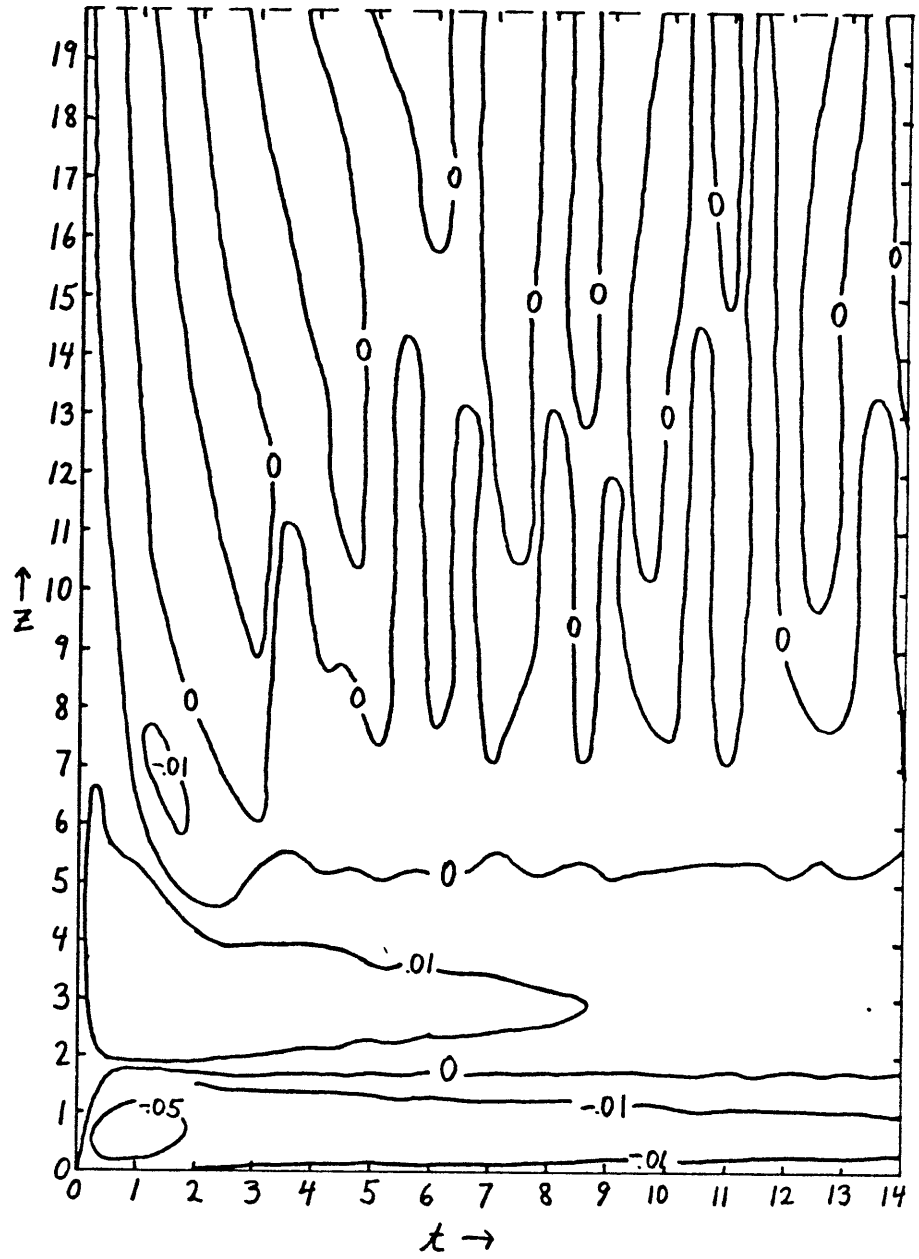

Figure 34. U Run 14, S = 2.56, H = 63.2 See p. 26.

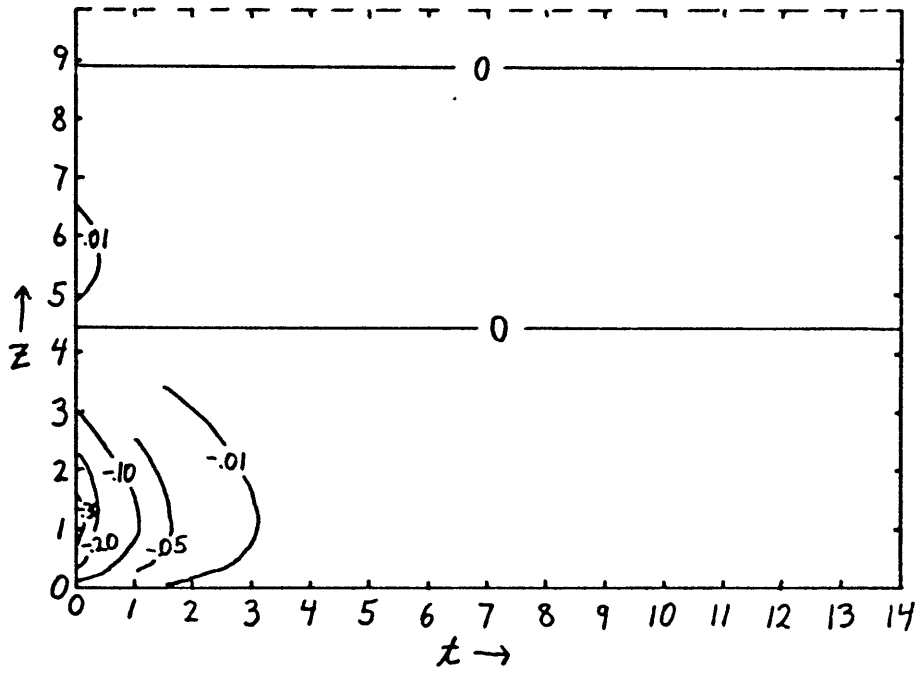

Figure 35. UEK Run 14, S = 2.56, H = 63.2 See p. 26.

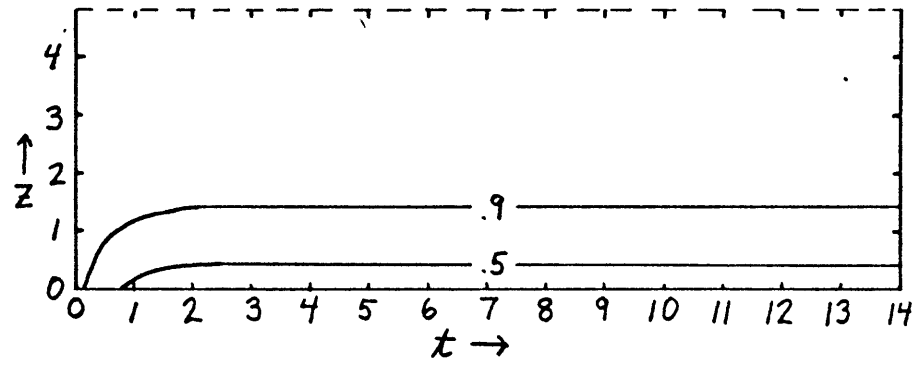

Figure 36. VQG Run 14, S = 2.56, H = 63.2 See p. 26.

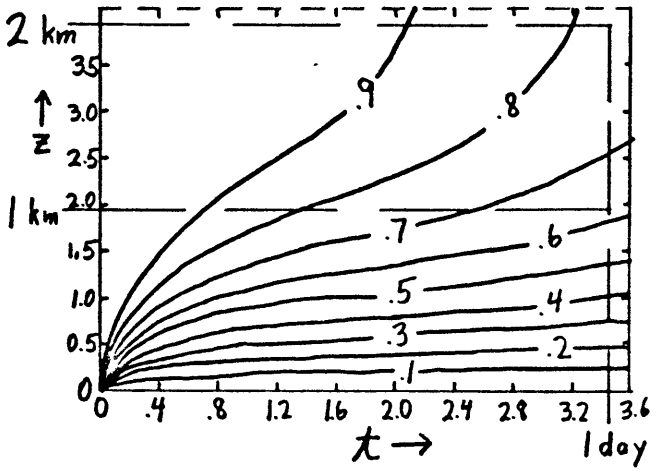

Figure 37. V Run 13, plotted dimensionally See p. 26.

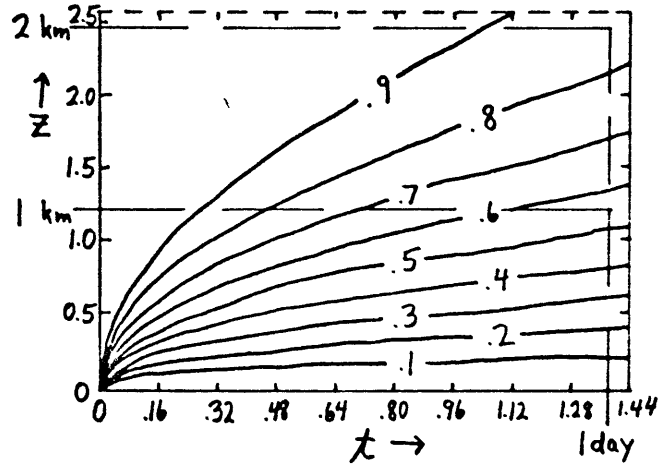

Figure 38. V Run 14, plotted dimensionally See p. 26.

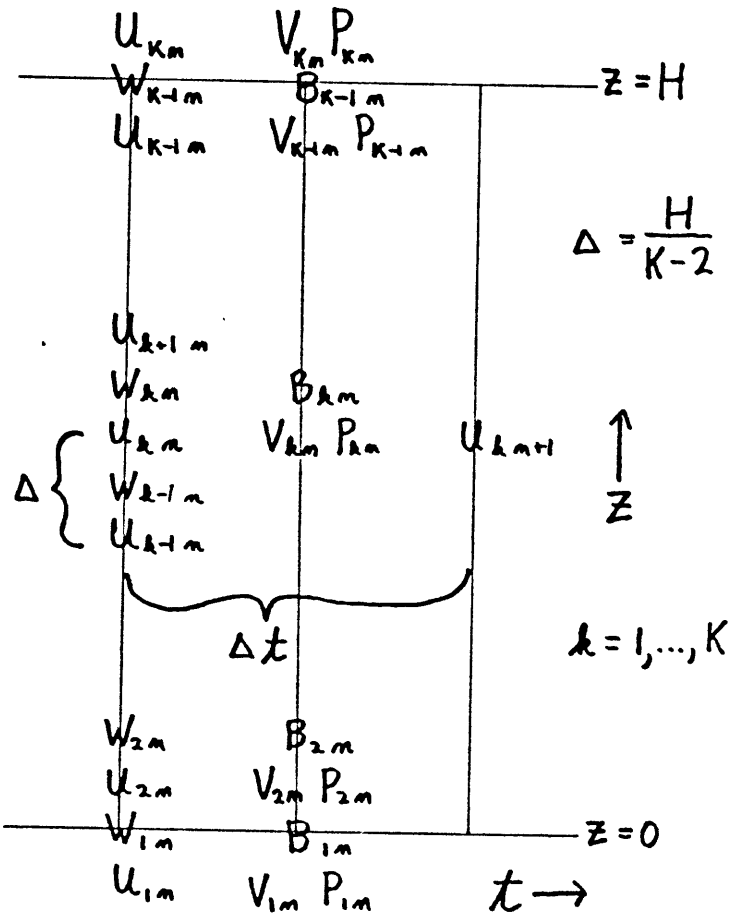

time increment = Δt, height increment = Δ

W_{Kn} and B_{Kn} are never used.

$V_{kn} = V(z = (k - 3/2)\Delta, t = n\Delta t)$

$B_{kn} = B(z = (k - 1)\Delta, t = n\Delta t)$

$P_{kn} = P(z = (k - 3/2)\Delta, t = n\Delta t)$

$U_{kn} = U(z = (k - 3/2)\Delta, t = (n - \frac{1}{2})\Delta t)$

$W_{kn} = W(z = (k - 1)\Delta, t = (n - \frac{1}{2})\Delta t)$

Figure 39. Finite difference grid for numerical model.

ACKNOWLEDGEMENTS

I would like to thank Professor Norman A. Phillips who suggested the problem and the numerical techniques, and who, as thesis advisor, provided continuing assistance and guidance until its completion. I would also like to thank John A. Young, visiting professor from the University of Wisconsin, for his valuable discussions of several aspects of the thesis.

While writing this thesis, I was supported by a National Science Foundation Graduate Fellowship. Some of the funds used for the research came from National Science Foundation Grant No. GA 28724x.

APPENDIX - Numerical Model

Numerical integrations of the complete equations (3-7) were conducted on a staggered, uniformly spaced grid in time and space. This grid is pictured in Figure 39. Because of the manipulations used in deriving (3-7), the resulting variables, U, V, W, P and B, are functions only of height (z) in space. The finite difference forms of the equations are then quite simple, being only one dimensional in space. Centered differencing techniques were used both in time and space. The resulting equations are:

$$(3)\longrightarrow \quad -U_{k+1\ n+1} + \alpha U_{k\ n+1} - U_{k-1\ n+1} = D_k, \qquad k = 2, \ldots, K-1$$

$$(7)\longrightarrow \quad W_{k\ n+1} = W_{k-1\ n+1} - \Delta U_{k\ n+1}, \qquad k = 2, \ldots, K-1$$

$$(5)\longrightarrow \quad -B_{k+1\ n+1} + \alpha B_{k\ n+1} - B_{k-1\ n+1} = G_k, \qquad k = 2, \ldots, K-2$$

$$(6)\longrightarrow \quad P_{k\ n+1} = P_{k-1\ n+1} + \Delta B_{k-1\ n+1}, \qquad k = 3, \ldots, K-1$$

$$(4)\longrightarrow \quad -V_{k+1\ n+1} + \alpha V_{k\ n+1} - V_{k-1\ n+1} = R_k, \qquad k = 1, \ldots, K$$

where:

$$D_k = U_{k+1\ n} - \beta U_{k\ n} + U_{k-1\ n} + \gamma(V_{k\ n} + P_{k\ n})$$

$$G_k = B_{k+1\ n} - \beta B_{k\ n} + B_{k-1\ n} - \gamma S W_{k\ n+1}$$

$$R_k = V_{k+1\ n} - \beta V_{k\ n} + V_{k-1\ n} - \gamma U_{k\ n-1}$$

$$\alpha = 2(1 + \Delta^2/\Delta t)$$

$$\beta = 2(1 - \Delta^2/\Delta t)$$

$$\gamma = 2\Delta^2$$

A technique devised by Richtmyer and Morton (1967, pp. 198-201) was used to solve the above U, V and B equations.

The equations were formulated to satisfy the boundary consitions (8). Because it is not possible to have infinite height in a numerical model, a vertical lid, at height z = H, was placed on the model at a height which hopefully was far enough away from the bottom boundary, so that it did not affect the motions near this boundary that were to be studied. Experiments were conducted to determine what H should be. The finite difference boundary conditions are:

At z = 0: $U_{1n} = -U_{2n}$ (no slip)

$V_{1n} = -V_{2n}$

$B_{1n} = W_{1n} = 0$

At z = H: $U_{Kn} = U_{K-1\ n}$ (slip)

$V_{Kn} = V_{K-1\ n}$

$B_{K-1\ n} = W_{K-1\ n} = 0$

W_{Kn} and B_{Kn} are never used.

At t = 0: $U_{k0} = W_{k0} = B_{k0} = 0$

$P_{k0} = -1$

$V_{k0} = 1$

Using the von Neumann necessary condition for stability, criteria were developed to ensure the stability of the numerical integration. The result was that both the following conditions must be satisfied simultaneously:

$$\Delta t \leq \frac{\Delta^2}{2} \qquad (22)$$

$$\Delta t < \frac{2}{\sqrt{1 + \frac{S H^2}{\pi^2}}} \qquad (23)$$

where: Δ = vertical grid increment

Δt = time increment

Condition (22) is more restrictive in all cases considered by at least an order of magnitude. The vertical grid increment was specified as $\Delta = 0.1$. This means that there were ten vertical grid points per Ekman depth. The time increment was then determined from (22):

$$\Delta = 0.1$$

$$\Delta t = 0.005$$

In most runs the integration was carried out 2800 time steps, until t = 14. This is the equivalent of one "e-folding" time for the case when S = 0.01, which was used as a standard case. One "e-folding" time is equal to $\sqrt{2/S}$.

REFERENCES

Barcilon, V., and J. Pedlosky, 1967a: Linear theory of rotating stratified fluid motions. J. Fluid Mech., 29, 1-16.

---, and ---, 1967b: A unified linear theory of homogeneous and stratified rotating fluids. J. Fluid Mech., 29, 609-621.

Benton, E.R., and A. Clark, Jr., 1974: Spin-up. Annual Reviews of Fluid Mechanics, 6, 257-280.

Greenspan, H.P., and L.N. Howard, 1963: On a time dependent motion of a rotating fluid. J. Fluid Mech., 17, 385-404.

Hildebrand, Francis B., 1962: Advanced Calculus for Applications, Englewood Cliffs, N.J., Prentice-Hall, Inc., 646pp.

Holton, J.R., 1965: The influence of viscous boundary layers on transient motions in a stratified rotating fluid: Part I. J. Atmos. Sci., 22, 402-411.

Richtmyer, R.D., and K.W. Morton, 1967: Difference Methods for Initial-Value Problems, New York, Interscience Publishers, 405 pp.

Young, J.A., 1973: A theory for isallobaric air flow in the planetary boundary layer. J. Atmos. Sci., 30, 1584-1592.